

# General-mass treatment for deep inelastic scattering at two-loop accuracy

Marco Guzzi,<sup>1</sup> Pavel M. Nadolsky,<sup>1</sup> Hung-Liang Lai,<sup>2</sup> C.-P. Yuan<sup>3,4</sup>

<sup>1</sup>*Department of Physics,  
Southern Methodist University,  
Dallas, TX 75275, USA*

<sup>2</sup>*Taipei Municipal University of Education,  
Taipei, Taiwan*

<sup>3</sup>*Department of Physics & Astronomy,  
Michigan State University,  
East Lansing, MI 48824, USA*

<sup>4</sup>*Center for High Energy Physics,  
Peking University, Beijing 100871, China*  
(Dated: August 25, 2011)

We present a next-to-next-to-leading order (NNLO) realization of a general quark mass scheme (S-ACOT- $\chi$ ) in deep inelastic scattering and explore the impact of NNLO terms on heavy-quark structure functions  $F_{2,L}^c(x, Q)$ . An amended QCD factorization theorem for DIS is discussed that validates the S-ACOT- $\chi$  scheme to all orders in the QCD coupling strength. As a new feature, kinematical constraints on collinear production of heavy quarks that are crucial near the heavy-quark threshold are included in the amended factorization theorem. An algorithmic procedure is outlined for implementing this scheme at NNLO by using mass-dependent and massless results from literature. At NNLO, the S-ACOT- $\chi$  scheme reduces scale dependence of heavy-quark DIS cross sections as compared to the fixed-flavor number scheme.

## I. INTRODUCTION

In a modern global QCD analysis of parton distribution functions (PDFs), several factors are comparable in magnitude to next-to-next-to-leading order (NNLO) radiative contributions in the QCD coupling strength  $\alpha_s$ . Among these factors, dependence of QCD cross sections on masses of heavy quarks,  $m_c$  and  $m_b$ , can be significant. Global fits are sensitive to two types of mass effects, kinematical suppression of production of  $c$  and  $b$  quarks near respective mass thresholds in deep inelastic scattering (DIS), and large radiative contributions to collinear production of  $c\bar{c}$  or  $b\bar{b}$  pairs at large collider energy. The first effect – suppression of DIS charm production near the threshold – must be carefully estimated when obtaining PDF parametrizations in order to accurately predict key scattering rates at the Large Hadron Collider [1]. The second effect is tied to an observation that  $c$  and  $b$  quarks behave as practically massless and indistinguishable from other massless flavors in typical Tevatron and LHC observables. It is therefore natural to evaluate all fitted cross sections in a “general-mass” (GM) factorization scheme, which assumes that the number of (nearly) massless quark flavors varies with energy, and at the same time includes dependence on heavy-quark masses in relevant kinematical regions.

In this paper, we study NNLO quark mass terms in the default GM scheme of CTEQ PDF analyses called “S-ACOT- $\chi$ ”. Since its inception in 1993 [2], the ACOT scheme has

undergone evolution based on the work in [3–5]. The S-ACOT- $\chi$  version of the ACOT scheme is employed successfully to compute heavy-quark cross sections in recent NLO CTEQ6.6, CT09, and CT10 global fits [6–8].

The S-ACOT- $\chi$  scheme is motivated by the QCD factorization theorem for DIS with massive quarks [3], which provides the scheme’s organizational backbone and key methods. In Sec. II, we demonstrate explicitly how to amend the QCD factorization theorem in order to validate the S-ACOT- $\chi$  scheme to all orders of  $\alpha_s$ . We then apply this scheme at NNLO to neutral-current DIS production, which provides the bulk of the DIS data, and for which all components of the calculation are readily available.<sup>1</sup>

Compared to other heavy-quark schemes available at NNLO [12–18], our implementation aims to achieve more explicit analogy to the computation of NNLO cross sections in the zero-mass (ZM) scheme [19–21]. As another distinction, the S-ACOT- $\chi$  scheme quickly converges to the fixed-flavor number scheme near the heavy-quark threshold as a consequence of the amended factorization theorem, without requiring supplemental matching conditions that are present in other general-mass schemes.

In Sec. II, the S-ACOT- $\chi$  cross sections are presented in the form that is reminiscent of counterpart ZM cross sections, up to replacement of some massless components by their mass-dependent expressions available in literature. This representation is based on a few compact formulas that include the desirable features existing in other heavy-quark NNLO calculations and lead to stable predictions for all scattering energies accessible. In Sec. III, numerical predictions are illustrated on the example of NNLO charm production cross sections. They show that inclusion of the NNLO terms reduces theoretical uncertainties compared to NLO.

Recent studies [1, 22–24] show that, at NLO, the LHC electroweak cross sections depend considerably on the mass scheme and parametric input for the charm mass  $m_c$  in the PDF analysis, even though the combined HERA-1 data set [25] itself has a small total uncertainty. Yet, the upcoming combination of HERA-1 heavy-quark cross sections is expected to improve constraints on  $m_c$ . The S-ACOT- $\chi$  implementation brings theoretical predictions up to matching accuracy by including the NNLO terms.

## II. S-ACOT- $\chi$ SCHEME: THEORETICAL FRAMEWORK

Consider neutral-current DIS at energy that is sufficient to produce  $N_l$  light flavors (such as  $l = u, d$  and  $s$ ) and one heavy flavor  $h$  (“charm”) with mass  $m_h$ . We postpone the straightforward extension to production of several heavy flavors until Sec. II D.

The GM scheme is designed so as to enable quick convergence of perturbative QCD series involving heavy quarks at any momentum transfer  $Q$ . Perturbative QCD cross sections in the GM scheme must converge reliably near the heavy-quark production threshold ( $Q^2 \approx m_h^2$ ), as well as far above it ( $Q^2 \gg m_h^2$ ), and smoothly interpolate between the limits. When  $Q$  is of order  $m_h$ , it is most natural to include all Feynman subgraphs with heavy-quark lines into the hard-scattering function (Wilson coefficient function). Such approach is called a “fixed-flavor number” (FFN) factorization scheme.  $\mathcal{O}(\alpha_s^2)$  coefficient functions for massive quark DIS production in this scheme have been computed in [26–28]. At this  $Q$ , the NNLO

---

<sup>1</sup> For charged-current DIS, only massless [9, 10] and some massive [11] NNLO coefficient functions have been computed.

coefficient functions in the GM scheme with  $N_l + 1$  flavors are expected to reduce to the FFN massive cross sections in the FFN scheme with  $N_l$  flavors. On the other hand, at high virtualities ( $Q^2 \gg m_h^2$ ), the NNLO GM cross sections should be indistinguishable from the NNLO ZM cross sections [19–21]. In this limit, the heavy-quark contributions are dominated by asymptotic collinear contributions that are also known to  $\mathcal{O}(\alpha_s^2)$  [12, 29–31].

A realization of such scheme called “ACOT” was developed in Refs. [2, 32] and proven for inclusive DIS to all orders in Ref. [3]. A non-zero PDF is assigned in this scheme to each quark flavor that can be physically produced at the given  $Q$ . The more recent S-ACOT- $\chi$  variant of the ACOT scheme adds two beneficial features. First, coefficient functions derived from Feynman graphs with initial-state heavy quarks are simplified by neglecting  $m_c$  dependence [3, 4]. Second, threshold suppression is introduced by evaluating these coefficient functions as a function of  $\chi \equiv x(1 + 4m_c^2/Q^2)$  instead of Bjorken  $x$  [5]. Both modifications follow from the factorization theorem for inclusive DIS [3] and produce predictions that are simpler, yet numerically accurate. They are included as a part of the NNLO implementation that is now presented.

### A. Overview of QCD factorization

A DIS structure function  $F(x, Q)$ , such as  $F_2$  or  $F_L$ , is written in a factorized form as

$$\begin{aligned} F(x, Q) &= \sum_{i=1}^{N_f^{fs}} e_i^2 \sum_{a=0}^{N_f} \int_x^1 \frac{d\xi}{\xi} C_{ia} \left( \frac{x}{\xi}, \frac{Q}{\mu}, \frac{m_h}{\mu}, \alpha_s(\mu) \right) \Phi_{a/p}(\xi, \mu) \\ &\equiv \sum_{i=1}^{N_f^{fs}} e_i^2 \sum_{a=0}^{N_f} [C_{ia} \otimes \Phi_{a/p}] (x, Q), \end{aligned} \quad (1)$$

where  $\Phi_{a/p}(\xi, \mu)$  is a parton distribution function (PDF) for a parton type  $a$ , light-cone momentum fraction  $\xi$ , and factorization scale  $\mu$ .  $C_{i,a}(\hat{x}, Q/\mu, m_h/\mu, \alpha_s(\mu))$  are Wilson coefficient functions evaluated at  $\hat{x} = x/\xi$ . Convolution integrals over  $\xi$  are indicated by “ $\otimes$ ”. Two sums appear on the right-hand side of Eq. (1), over all quark flavors  $i = 1, \dots, N_f^{fs}$  that couple to the virtual photon with fractional electric charges  $e_i = 2/3$  or  $-1/3$ , and over parton flavors  $a$  in the PDF  $\Phi_{a/p}$ . The index  $a$  runs over quark flavors ( $a = 1, \dots, N_f$  for  $u, d, s, \dots$ ) and the gluon ( $a = 0$ ). Perturbative coefficients of neutral-current DIS are the same for quarks and antiquarks up to NNLO. For each combination of flavors  $i$  and  $a$ , summation of quark and antiquark contributions of these flavors is always implied, but not shown for brevity.

Eq. (1) distinguishes between  $N_f^{fs}$ , the number of quark flavors produced in the final state ( $fs$ ), and  $N_f$ , the number of active quark flavors in  $\alpha_s$  and PDFs. The distinction is important for the ensuing discussion, as generally  $N_f^{fs}$  is different from  $N_f$  [1].  $N_f^{fs}$  is equal to the number of final-state flavors that can be produced at the given  $\gamma^*p$  center-of-mass energy  $W = Q\sqrt{1/x - 1}$ . All produced quark states can couple to the photon, so that the outer summation in Eq. (1) runs up to  $i = N_f^{fs}$ .

On the other hand,  $N_f$  is a parameter of the renormalization and factorization schemes. It is commonly set equal to the number of quark flavors with masses lighter than  $Q$ . Only flavors with  $a \leq N_f$  have non-zero PDFs in the inner summation, but their actual number depends on the factorization scheme.

To determine  $C_{i,a}$ , we calculate auxiliary structure functions for scattering on an initial-state parton  $b$ ,  $F(e + b \rightarrow e + X) \equiv \sum_{i=1}^{N_f^{fs}} e_i^2 F_{i,b}$ . The coefficient functions  $C_{i,a}$  are infrared-safe parts of  $F_{i,b}$ . They enter convolutions together with parton-level PDFs  $\Phi_{a/b}(\xi, \mu)$  for splittings  $b \rightarrow a$ , as

$$F_{i,b}(\hat{x}, Q) = \sum_{a=1}^{N_f} [C_{i,a} \otimes \Phi_{a/b}] (\hat{x}, Q). \quad (2)$$

In the  $\overline{\text{MS}}$  scheme, the parton-level PDFs are given by matrix elements of bilocal field operators that can be computed in perturbation theory. For example, the PDF for finding a quark  $q$  in a massless parton  $b$ , in the light-like gauge, is

$$\Phi_{q/b}(\xi) = \int \frac{dy^-}{2\pi} e^{-\xi p^+ y^-} \langle b(p) | \bar{\psi}(0, y^-, \vec{0}_T) \gamma^+ \psi(0) | b(p) \rangle, \quad (3)$$

where the light-cone momentum components of the partons  $b$  and  $q$  are  $p^\mu = \{p^+, 0, \vec{0}_T\}$  and  $k^\mu = \{\xi p^+, m_q^2/(2\xi p^+), \vec{0}_T\}$ , respectively, and  $p^\pm \equiv (p^0 \pm p^3)/\sqrt{2}$ .

The functions  $F_{i,b}$ ,  $C_{i,a}$ , and  $\Phi_{a/b}$  can be expanded as a series of  $a_s \equiv \alpha_s(\mu, N_f)/(4\pi)$ :

$$F_{i,b}(x) = F_{i,b}^{(0)}(x) + a_s F_{i,b}^{(1)}(x) + a_s^2 F_{i,b}^{(2)}(x) + \dots, \quad (4)$$

$$C_{i,a}(\hat{x}) = C_{i,a}^{(0)}(\hat{x}) + a_s C_{i,a}^{(1)}(\hat{x}) + a_s^2 C_{i,a}^{(2)}(\hat{x}) + \dots, \quad (5)$$

$$\Phi_{a/b}(\xi) = \delta_{ab} \delta(1 - \xi) + a_s A_{ab}^{(1)}(\xi) + a_s^2 A_{ab}^{(2)}(\xi) + \dots \quad (6)$$

In the last equation,  $A_{ab}^{(k)}$  ( $k = 0, 1, 2, \dots$ ) are perturbative coefficients composed of DGLAP splitting functions  $P_{ab}^{(k)}$ , such as  $A_{hg}^{(1)}(\xi) = 2 P_{hg}^{(1)}(\xi) \ln(\mu^2/m_h^2)$  for the  $g \rightarrow h\bar{h}$  splitting.

By equating coefficients on both sides of Eq. (2), order by order in  $a_s$ , we obtain

$$\begin{aligned} C_{i,b}^{(0)}(\hat{x}) &= F_{i,b}^{(0)}(\hat{x}), \\ C_{i,b}^{(1)}(\hat{x}) &= F_{i,b}^{(1)}(\hat{x}) - [C_{i,a}^{(0)} \otimes A_{ab}^{(1)}](\hat{x}), \\ C_{i,b}^{(2)}(\hat{x}) &= F_{i,b}^{(2)}(\hat{x}) - [C_{i,a}^{(0)} \otimes A_{ab}^{(2)}](\hat{x}) - [C_{i,a}^{(1)} \otimes A_{ab}^{(1)}](\hat{x}). \end{aligned} \quad (7)$$

Perturbative terms  $C_{i,a}^{(k)}$  in the coefficient functions are thus derived from perturbative expansions for  $F_{i,b}$  and  $\Phi_{a/b}$ , upon implied summation over the repeating index  $a$ .

The coefficients  $A_{ab}^{(k)}$  in  $\Phi_{a/b}$  consist of large or singular terms arising in  $F_{i,b}^{(k)}$  when the momenta of  $a$  and  $b$  are collinear. Subtraction of convolutions of the  $A_{ab}^{(k)}$  terms from  $F_{i,b}^{(k)}$  on the right-hand side of Eqs. (7) produces a finite (infrared-safe) result.

Depending on masses of  $a$  and  $b$ , two forms of  $A_{ab}^{(k)}$  in these equations are possible. If both  $a$  and  $b$  are massless,  $A_{ab}^{(k)}$  contains a singular part, given in  $n = 4 - \epsilon$  dimensions by  $\sum_{p=0}^k (1/\epsilon)^p s_{p,ab}$ , where  $s_{p,ab}$  contains a DGLAP splitting function; and a finite part (logs+finite terms) of the form  $\sum_{p=0}^k \ln^p(\mu^2/\mu_{IR}^2) s'_{p,ab}$ , where  $\mu$  is the factorization scale, and  $\mu_{IR}$  is the parameter of dimensional regularization in the infrared limit.

When these “mass singularities” are subtracted as in Eq. (7), one obtains infrared-safe parts  $\widehat{F}_{i,b}^{(k)}$  of  $F_{i,b}^{(k)}$ , denoted by a caret:

$$\widehat{F}_{i,b}^{(k)}\left(\widehat{x}, \frac{Q^2}{\mu^2}\right) = F_{i,b}^{(k)}\left(\widehat{x}, \frac{Q^2}{\mu_{IR}^2}, \frac{1}{\epsilon}\right) - \sum_{p=0}^k \left[ C_{i,a}^{(p)} \otimes A_{ab}^{(k-p)} \right] \left(\widehat{x}, \frac{\mu^2}{\mu_{IR}^2}, \frac{1}{\epsilon}\right). \quad (8)$$

The difference  $\widehat{F}_{i,b}^{(k)}$  is finite, even though both the “bare” functions  $F_{i,b}^{(k)}$  and the PDF coefficients  $A_{ab}^{(k)}$  contain the singular  $1/\epsilon^p$  terms, where  $p$  is a positive integer.

If a massive parton  $a$  is produced from a massless parton  $b$  (as in  $g \rightarrow c\bar{c}$  or  $u \rightarrow g \rightarrow c\bar{c}$ ), the coefficients  $A_{ab}^{(k)}$  consist solely of logarithms and finite terms involving mass  $m_a$ ,

$$A_{ab}^{(k)}\left(\xi, \frac{\mu^2}{m_a^2}\right) = \sum_{p=0}^k \ln^p(\mu^2/m_a^2) s'_{p,ab}(\xi). \quad (9)$$

The coefficient  $A_{ab}^{(k)}$  is finite for  $m_a \neq 0$ , but  $A_{ab}^{(k)} \rightarrow \infty$  when  $\mu^2 \gg m_a^2$ . For such massive quarks, the coefficients  $A_{ab}^{(k)}$  appear as subtractions from massive  $F_{ib}^{(k)}$  in expressions for  $C_{i,a}^{(k)}$ . In accordance with the S-ACOT scheme, mass-dependent  $A_{ab}^{(k)}$  only appear in explicit heavy-particle production, *i.e.*, when transitions  $b(m_b = 0) \rightarrow a(m_a \neq 0)$  are involved. All other subprocesses use massless expressions, constructed from renormalized parts  $\widehat{F}_{i,b}^{(k)}\left(x, \frac{Q}{\mu}\right)$  given by Eq. (8).

## B. Heavy-quark component $F_h$ of inclusive $F(x, Q)$

To construct the Wilson coefficient functions explicitly, we decompose  $F(x, Q)$  according to the (anti-)quark couplings to the photon [18]. Terms in which the photon couples to the light ( $l$ ) or heavy ( $h$ ) quark are designated as  $F_l$  and  $F_h$ , respectively:

$$F = \sum_{l=1}^{N_l} F_l + F_h, \quad (10)$$

with

$$F_l(x, Q) = e_l^2 \sum_a \left[ C_{l,a} \otimes \Phi_{a/p} \right] (x, Q), \quad (11)$$

and

$$F_h(x, Q) = e_h^2 \sum_a \left[ C_{h,a} \otimes \Phi_{a/p} \right] (x, Q). \quad (12)$$

Note that this separation is purely theoretical:  $F_l$  and  $F_h$  cannot be measured separately or distinguished in another way. Furthermore, the heavy-quark component  $F_h$  is not the same as the semi-inclusive heavy-quark structure function  $F_{h,SI}$  measured in experiments. The relation between  $F_{h,SI}$  and  $F_h$  is clarified in Sec. IID, with the explicit formula given by Eq. (41).

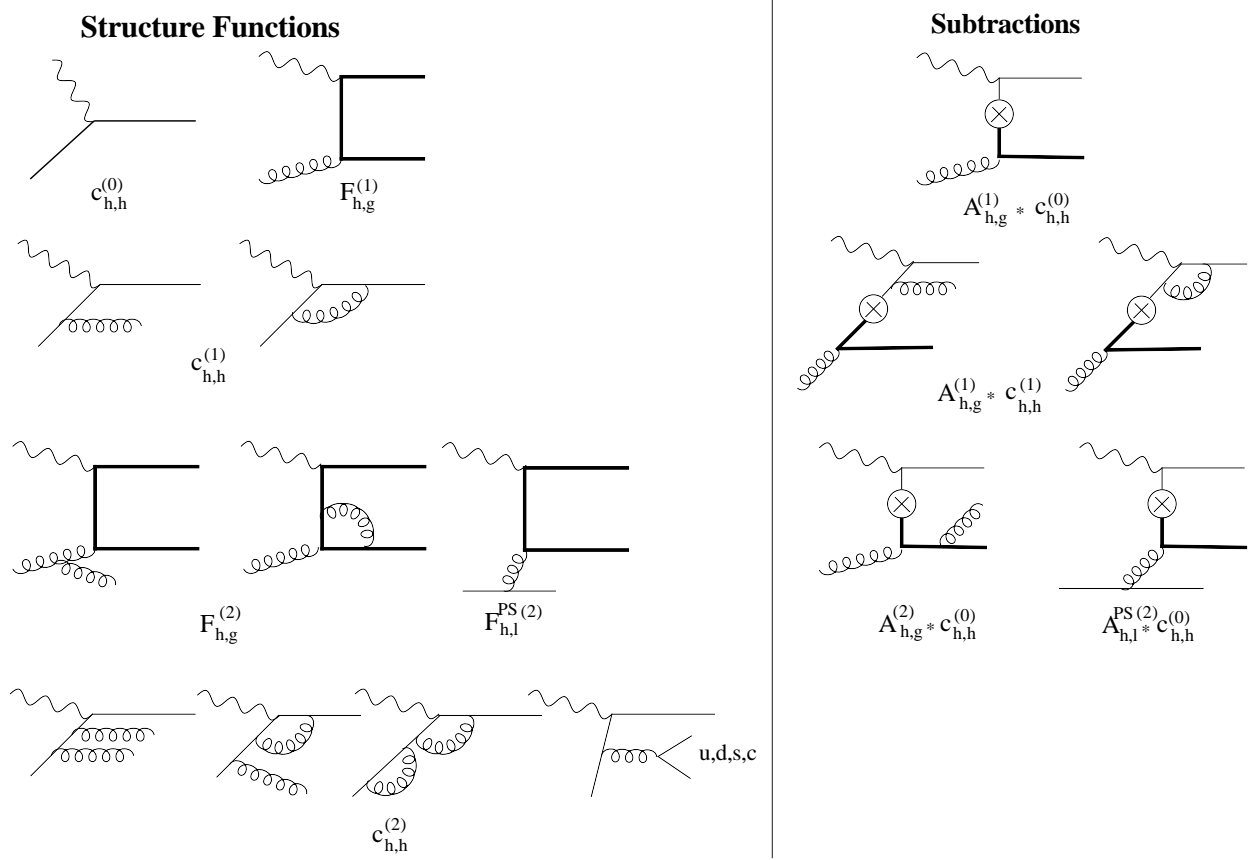


FIG. 1: Representative scattering contributions to  $F_h(x, Q)$ .

Concentrating first on the contribution  $F_h$  with the photon coupled to  $h$ , we obtain its Wilson coefficients  $C_{h,a}(\hat{x})$  from the parton-level functions  $F_{h,b}$  via Eqs. (7):

$$\begin{aligned}
 C_{h,a}^{(0)}(\hat{x}) &= \delta_{ha} \delta(1 - \hat{x}); \\
 C_{h,g}^{(1)} &= F_{h,g}^{(1)} - C_{h,h}^{(0)} \otimes A_{hg}^{(1)}; \quad C_{h,l}^{(1)} = C_{l,h}^{(1)} = 0; \quad C_{h,h}^{(1)} = F_{h,h}^{(1)} - C_{h,h}^{(0)} \otimes A_{hh}^{(1)}; \\
 C_{h,g}^{(2)} &= F_{h,g}^{(2)} - C_{h,h}^{(0)} \otimes A_{hg}^{(2)} - C_{h,h}^{(1)} \otimes A_{hg}^{(1)} - C_{h,g}^{(1)} \otimes A_{gg}^{(1)}; \\
 C_{h,l}^{(2)} &= F_{h,l}^{PS,(2)} - C_{h,h}^{(0)} \otimes A_{hl}^{PS,(2)} - C_{h,g}^{(1)} \otimes A_{gl}^{(1)}; \\
 C_{h,h}^{(2)} &= F_{h,h}^{(2)} - C_{h,h}^{(0)} \otimes A_{hh}^{(2)} - C_{h,h}^{(1)} \otimes A_{hh}^{(1)} - C_{h,g}^{(1)} \otimes A_{gh}^{(1)}.
 \end{aligned} \tag{13}$$

In these expressions, the coefficient  $C_{h,l}^{(2)}$  with the initial-state light quark depends on flavor-non-diagonal, or pure-singlet (PS), components of  $F_{i,j}^{(2)}$  and  $A_{ij}^{(2)}$ , defined by

$$G_{i,j} \equiv G_{i,j}^{PS} + \delta_{ij} G_{i,j}^{NS}, \text{ for } G_{i,j} = C_{i,j}^{(2)}, F_{i,j}^{(2)}, \text{ and } A_{i,j}^{(2)}. \tag{14}$$

On the other hand, the coefficient  $C_{h,h}^{(2)}$  with the initial-state heavy quark depends both on the pure singlet (PS) and non-singlet (NS) components, as will be shown below.

Representative diagrams for heavy-quark contributions in Eqs. (13) are shown in Fig. 1. The reader may consult this figure frequently to identify various terms in the ensuing discussion. Propagators and external legs for quarks that are indicated by thick lines (thin lines) will eventually be computed with full mass dependence (in the massless approximation).



The heavy-quark diagrams fall into two categories, those that do not involve a collinear approximation for scattering of heavy quarks (often called “flavor-creation”, or FC, terms), and those that do (flavor-excitation, or FE, terms). While FC contributions must be evaluated exactly, the approximate nature of the FE terms allows some useful simplifications.

At  $\mathcal{O}(\alpha_s^2)$ , the flavor-creation contributions include the coefficients  $F_{h,g}^{(1)}$ ,  $F_{h,g}^{(2)}$ , and  $F_{h,l}^{PS,(2)}$ . The heavy quarks appear in these terms inside the  $O(\alpha_s)$  Feynman subgraph for  $\gamma^* g \rightarrow h\bar{h}$ , connected by a gluon propagator to an initial-state gluon or a light quark. These contributions are evaluated with the exact kinematical dependence on  $m_h$ , and hence are defined unambiguously.

The FE cross sections are proportional to the heavy-quark PDF that approximates collinear production of heavy-quark pairs from light partons in the high-energy limit. Structure functions and coefficient functions with an initial-state heavy quark, such as  $F_{h,h}^{(k)}$  and  $C_{h,h}^{(k)}$ , fall into this class. The FE coefficient functions reduce to unique  $\overline{\text{MS}}$  expressions when  $m_h$  is negligible [3], but, near the threshold, they may differ by non-unique powerlike contributions  $(m_h^2/Q^2)^p$  with  $p > 0$ . Within the ACOT scheme, several conventions have been proposed to include the powerlike contributions in a way compatible with the QCD factorization theorem.<sup>2</sup>

Among these conventions, the “full ACOT scheme” [2] evaluates the FE coefficient functions ( $C_{h,h}^{(k)}$ , etc.) with their complete mass dependence. The simplified ACOT (S-ACOT) scheme [3, 4] neglects *all* mass terms in  $C_{h,h}^{(k)}$  and thereupon reduces tedious computations typical for the full ACOT scheme. The S-ACOT- $\chi$  scheme [5] adopted in our computation includes *the most important* mass dependence in  $C_{h,h}^{(k)}$  and uses simpler zero-mass expressions everywhere else.

If we denote the mass-dependent and massless quantities by uppercase and lowercase letters, and renormalized ZM functions by a caret, the S-ACOT- $\chi$  convention for functions with initial-state heavy quarks is summarized as

$$C_{h,h}^{(k)}\left(\frac{x}{\xi}, \frac{Q}{\mu}, \frac{m_h}{Q}\right) = c_{h,h}^{(k)}\left(\frac{\chi}{\xi}, \frac{Q}{\mu}, m_h = 0\right) \theta(\chi \leq \xi \leq 1), \quad (15)$$

and

$$F_{h,h}^{(k)}\left(\frac{x}{\xi}, \frac{Q}{\mu}, \frac{m_h}{Q}\right) = \hat{f}_{h,h}^{(k)}\left(\frac{\chi}{\xi}, \frac{Q}{\mu}, m_h = 0\right) \theta(\chi \leq \xi \leq 1), \quad (16)$$

where

$$\chi = x \left(1 + \frac{4m_h^2}{Q^2}\right). \quad (17)$$

This form reflects an observation that the largest powerlike terms are associated with the constraint on the integration range in the convolution that reflects energy conservation in production of massive heavy-quark pairs [33]. This is practically achieved by evaluating ZM functions with  $\chi$  instead of Bjorken  $x$  as an input parameter, and by constraining the momentum fraction in the FE channels to be in the range  $\chi \leq \xi \leq 1$ . Justification for the  $\chi$  convention in the context of the proof of the QCD factorization is presented in Sec. II E. Its numerical impact is discussed in Sec. III E.

---

<sup>2</sup> The differences between these conventions are formally of a higher order in  $\alpha_s$ , but some conventions lead to faster perturbative convergence.

When the S-ACOT- $\chi$  scheme is adopted, Eqs. (13) become

$$c_{h,a}^{(0)} = \delta_{ha} \delta(1 - \hat{\chi}); \quad c_{h,h}^{(1)} = \hat{f}_{h,h}^{(1)}; \quad (18)$$

$$C_{h,g}^{(1)} = F_{h,g}^{(1)} - A_{hg}^{(1)}; \quad (19)$$

$$C_{h,g}^{(2)} = \hat{F}_{h,g}^{(2)} - A_{hg}^{(2)} - c_{h,h}^{(1)} \otimes A_{hg}^{(1)}; \quad (20)$$

$$c_{h,h}^{(2)} = \hat{f}_{h,h}^{(2)}; \quad C_{h,l}^{(2)} = \hat{F}_{h,l}^{PS,(2)} - A_{hl}^{PS,(2)}. \quad (21)$$

Lowercase functions on the right-hand side of these equations are given by ZM expressions. Among all terms, only the structure functions  $F_{h,g}^{(1)}$ ,  $\hat{F}_{h,g}^{(2)}$ , and  $\hat{F}_{h,l}^{PS,(2)}$  are calculated with the exact mass dependence. The carets above  $\hat{F}_{h,g}^{(2)}$  and  $\hat{F}_{h,l}^{PS,(2)}$  indicate that the massless pole terms,  $C_{h,g}^{(1)} \otimes A_{gg}^{(1)}$  and  $C_{h,g}^{(1)} \otimes A_{gl}^{(1)}$ , are subtracted from them.

In the rest of the terms, the input longitudinal variable is set to be  $\hat{\chi} = \chi/\xi$ . The convolution of any such term  $f(\hat{\chi})$  with the PDF  $\Phi(\xi)$  is

$$[f \otimes \Phi](\zeta) \equiv \int_{\zeta}^1 \frac{d\xi}{\xi} f\left(\frac{\zeta}{\xi}\right) \Phi(\xi), \quad (22)$$

where  $\zeta = \chi$ . [The naive massless approximation is  $\zeta = x$ .]

The one-loop expressions  $\hat{f}_{h,h}^{(k)}$ ,  $F_{h,g}^{(1)}$ , and  $A_{hg}^{(1)}$  can be found in [2, 12, 34].  $\hat{F}_{h,g}^{(2)}$  and  $\hat{F}_{h,l}^{PS,(2)}$  coincide with the massive structure functions with initial-state gluons and pure-singlet light quarks in [26, 27]. They are independent of  $N_l$ . The expressions for  $A_{hg}^{(2)}$  and  $A_{hl}^{(2)}$  are computed as  $A_{Hg}^{(2)}$  and  $A_{Hq}^{(2)}$  in [12].

The  $\mathcal{O}(\alpha_s^2)$  contribution  $c_{h,h}^{(2)} = \hat{f}_{h,h}^{(2)}$  corresponds to radiation of up to  $N_l + 1$  flavors of  $q\bar{q}$  pairs off an incoming quark  $h$ . It can be found as a sum of the pure-singlet and non-singlet ZM coefficient functions from Refs. [19–21, 35, 36]:

$$c_{h,h}^{(2)} = c_{h,h}^{PS,(2)} + c_{h,h}^{NS,(2)} = \hat{f}_{h,h}^{(2)} = \hat{f}_{h,h}^{PS,(2)} + \hat{f}_{h,h}^{NS,(2)}. \quad (23)$$

In this equation, both pure-singlet and non-singlet parts of  $\hat{f}_{h,h}^{(2)}$  are taken to be massless, which is one of the choices possible within the S-ACOT scheme. It is equally acceptable to evaluate the pure-singlet  $F_{h,h}^{PS,(2)}$  with full mass dependence, so that the corresponding coefficient function is given by the massive  $C_{h,l}^{(2)}$  in Eq. (21). In this case,  $F_{h,h}^{PS,(2)}$  can be combined with the pure-singlet contribution with initial-state light quarks, also given by  $C_{h,l}^{(2)}$ .

The complete  $\mathcal{O}(\alpha_s^2)$  part of  $F_h(x, Q)$  then takes the form

$$F_h^{(2)} = e_h^2 \left\{ c_{h,h}^{NS,(2)} \otimes (\Phi_{h/p} + \Phi_{\bar{h}/p}) + C_{h,l}^{(2)} \otimes \Sigma + C_{h,g}^{(2)} \otimes \Phi_{g/p} \right\}, \quad (24)$$

where  $\Sigma(x, \mu)$  is the singlet quark PDF summed over  $N_f = N_l + 1$  flavors:

$$\Sigma(x, \mu) = \sum_{i=1}^{N_f} [\Phi_{i/p}(x, \mu) + \Phi_{\bar{i}/p}(x, \mu)]. \quad (25)$$

We use Eq. (24) for practical implementation of  $F_h$ , with the coefficient functions computed as in Eqs. (20) and (21).



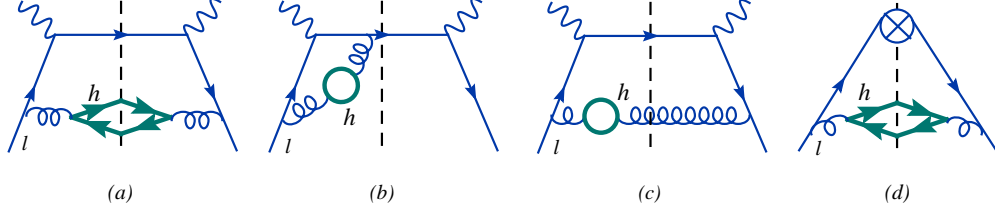


FIG. 2: Disconnected heavy-quark contributions to  $F_{l,l}^{NS,(2)}$  (a,b,c) and  $A_{l,l}^{NS,(2)}$  (d).

### C. Light-quark component of $F(x, Q)$

By a similar argument, Eq. (7) serves as a starting point for finding coefficient functions for the light-quark component  $F_l(x, Q)$ . The corresponding Wilson coefficients are

$$\begin{aligned}
 c_{l,a}^{(0)} &= \delta_{la} \delta(1-x); \\
 C_{l,l}^{(1)} &= F_{l,l}^{(1)} - C_{l,l}^{(0)} \otimes A_{ll}^{(1)}; \quad C_{l,g}^{(1)} = F_{l,g}^{(1)} - C_{l,l}^{(0)} \otimes A_{lg}^{(1)}; \quad C_{l,h}^{(1)} = C_{l,l'}^{(1)} = 0; \\
 C_{l,l}^{(2)} &= F_{l,l}^{PS,(2)} + F_{l,l}^{NS,(2)} - C_{l,l}^{(0)} \otimes [A_{ll}^{PS,(2)} + A_{ll}^{NS,(2)}] - C_{l,l}^{(1)} \otimes A_{ll}^{(1)} - C_{l,g}^{(1)} \otimes A_{gl}^{(1)}; \\
 C_{l,l'}^{(2)} &= F_{l,l'}^{PS,(2)} - C_{l,l}^{(0)} \otimes A_{ll'}^{PS,(2)} - C_{l,g}^{(1)} \otimes A_{gl'}^{(1)}; \\
 C_{l,h}^{(2)} &= F_{l,h}^{PS,(2)} - C_{l,l}^{(0)} \otimes A_{lh}^{PS,(2)} - C_{l,g}^{(1)} \otimes A_{gh}^{(1)}; \\
 C_{l,g}^{(2)} &= F_{l,g}^{(2)} - C_{l,l}^{(0)} \otimes A_{lg}^{(2)} - C_{l,l}^{(1)} \otimes A_{lg}^{(1)} - C_{l,g}^{(1)} \otimes A_{gg}^{(1)}.
 \end{aligned} \tag{26}$$

The quark-to-quark Wilson coefficients  $C_{l,l}^{(2)}$ ,  $C_{l,h}$ , and  $C_{l,l'}^{(2)}$  (for  $l' \neq l$ ) are decomposed into their PS and NS components as in Eq. (14). Non-singlet contributions  $F_{l,l}^{NS,(2)}$  and  $A_{ll}^{NS,(2)}$  contain squared matrix elements with heavy-quark lines that are disconnected from the initial-state proton, as in Fig. 2. These diagrams must be evaluated with full dependence on  $m_h$ . The rest of the coefficients in Eqs. (26) do not contain disconnected heavy-quark lines. They are evaluated by ZM formulas.

Explicitly, the non-singlet functions with mass dependence consist of two parts, arising either from Feynman diagrams with light partons only (designated as  $g_{light}$ ), or with a heavy quark in the final-state emission or virtual loop (denoted by  $G_{heavy}(m_h)$ ):

$$G = g_{light} + G_{heavy}(m_h),$$

where  $G = F_{l,l}^{NS,(2)}$  or  $A_{ll}^{NS,(2)}$ . The function  $g_{light}$  is evaluated in the ZM approximation, while  $G_{heavy}(m_h)$  retains complete  $m_h$  dependence. Masses can be neglected in the rest of Eqs. (26), so we get

$$c_{l,a}^{(0)} = \delta_{la} \delta(1-x); \tag{27}$$

$$c_{l,l}^{(1)} = \hat{f}_{l,l}^{(1)}; \quad c_{l,g}^{(1)} = \hat{f}_{l,g}^{(1)}; \quad c_{l,h}^{(1)} = c_{l,l'}^{(1)} = 0; \tag{28}$$

$$C_{l,l}^{(2)} = C_{l,l}^{NS,(2)} + c^{PS,(2)}, \quad \text{where} \tag{29}$$

$$C_{l,l}^{(2),NS} = \hat{f}_{l,l,light}^{NS,(2)} + F_{l,l,heavy}^{NS,(2)} - A_{ll,heavy}^{NS,(2)}; \tag{30}$$

$$c_{l,h}^{(2)} = c_{l,l'}^{(2)} = c^{PS,(2)}; \quad c_{l,g}^{(2)} = \hat{f}_{l,g}^{(2)}. \tag{31}$$

The 1-loop coefficients  $c_{l,a}^{(1)}$  are well-known from Refs. [37–39]. The 2-loop massless contributions in Eqs. (30) and (31) can be derived from the published ZM results according to the following procedure. Using the decomposition Eq. (14) for  $c_{i,j}$  in the ZM scheme,

$$c_{i,j} \equiv c^{PS} + \delta_{ij} c^{NS,(2)}, \quad (32)$$

where  $c^{PS}$  and  $c^{NS}$  are independent of the quark flavors  $i$  or  $j$  given that the masses are neglected, we write

$$\begin{aligned} F(x, Q) &= \sum_{i,a} e_i^2 [c_{i,a} \otimes \Phi_{a/p}] = \sum_i e_i^2 \left\{ \sum_j (c^{PS} + \delta_{ij} c^{NS}) \otimes \Phi_{j/p} + c_g \otimes \Phi_{g/p} \right\} \\ &= [c^{NS} \otimes \Sigma^{+,NS}] + \frac{(\sum_i e_i^2)}{N_f} \{ [c^S \otimes \Sigma] + N_f [c_g \otimes \Phi_{g/p}] \}. \end{aligned} \quad (33)$$

Here

$$c^S \equiv c^{NS} + N_f c^{PS}.$$

The singlet PDF  $\Sigma(x, \mu)$  is given by Eq. (25), and the non-singlet sum of (anti-)quark PDFs is

$$\Sigma^{+,NS}(x, \mu) = \sum_{i=1}^{N_f} e_i^2 \left( \Phi_{i/p}(x, \mu) + \Phi_{\bar{i}/p}(x, \mu) - \frac{1}{N_f} \Sigma(x, \mu) \right).$$

Eq. (33) expresses  $F(x, Q)$  in the same representation as Eq. (4.1) in the N<sup>3</sup>LO calculation of DIS cross sections [36]. Comparing Eqs. (30) and (31) with ZM coefficient functions in Section 4 of that reference (which are indicated here by an asterisk “\*”), we find that

$$c^{PS,(2)} = c_{I,ps}^{(2,*)}/N_f, \quad (34)$$

$$\hat{f}_{i,g}^{(2)} = c_{I,g}^{(2,*)}/N_f, \quad (35)$$

and

$$\hat{f}_{l,l,heavy}^{NS,(2)} = c_{I,ns}^{(2,*)}(n_f = N_l), \quad (36)$$

with  $I = 2$  or  $L$  for  $F_2(x, Q)$  and  $F_L(x, Q)$ , respectively.

The non-singlet heavy-quark coefficient function,

$$F_{l,l,heavy}^{NS,(2)}(x, Q^2/m_h^2) = \left( L_{I,q}^{NS,(2)}(x, Q^2/m_h^2) \right)_+ + \frac{2}{3} \ln \left( \frac{Q^2}{m_h^2} \right) c_{l,l}^{(1)}(x), \quad (37)$$

is composed of contributions of several classes shown in Figs. 2(a)-(c). Diagrams with real emission of a heavy-quark pair (as in Fig. 2(a)) in  $F_I(x, Q)$  contribute a function  $L_{I,q}^{NS,(2)}(x, Q^2/m_h^2)$  in Eqs. (A.1) and (A.2) of Ref. [40]. This contribution is combined with the virtual two-loop diagrams, cf. Fig. 2(b), to produce the first term on the right-hand side of Eq. (37), in which  $L_{I,q}^{NS,(2)}(x, Q^2/m_h^2)$  is regularized by the plus prescription at  $x \rightarrow 1$ . Contributions with a heavy-quark polarization graph inserted into a one-loop  $\gamma^* q$  scattering diagram, of the kind shown in Fig. 2(c), produce the second term in Eq. (37), where  $c_{l,l}^{(1)}$  is available from Refs. [37–39].

In this derivation, we do not explicitly compute the virtual loop contribution in Fig. 2(b), but deduce it from the Adler sum rule [41–44]. The sum rule states that the sum of the real and virtual contributions to  $F_{l,l,heavy}^{NS,(2)}(x, Q^2/m_h^2)$  satisfies

$$\int_0^1 F_{l,l,heavy}^{NS,(2)}(x, Q^2/m_h^2) dx = 0. \quad (38)$$

With this rule, it can be demonstrated that the virtual contribution amounts to imposing the plus prescription on  $L_{I,q}^{NS,(2)}(x, Q^2/m_h^2)$  as in Eq. (37).

In the asymptotic limit  $Q^2 \gg m_h^2$ ,  $F_{l,l,heavy}^{NS,(2)}$  for the inclusive  $F_2$  contains large terms proportional to  $\ln(Q^2/m_h^2)$ . Those coincide with the  $\mathcal{O}(\alpha_s^2)$  non-singlet part  $A_{l,l,heavy}^{NS,(2)}$  of the light-quark PDF that includes radiation of a heavy-quark pair as shown in Fig. 2(d).  $A_{l,l,heavy}^{NS,(2)}$  is computed as  $A_{qq,H}^{NS,(2)}(z, m_h^2/\mu^2)$  in Eq. (B.4) of Ref. [12], which we evaluate as a function of  $z = \chi/\xi$  in accord with the S-ACOT- $\chi$  scheme.

When  $A_{l,l,heavy}^{NS,(2)}$  is subtracted from  $F_{l,l,heavy}^{NS,(2)}$  as in Eq. (30), the difference is free of the collinear logs. After the difference is combined with the light-quark-only contributions  $\hat{f}_{l,l,tight}^{NS,(2)}$ , we obtain the full non-singlet coefficient function  $C_{l,l}^{(2),NS}$ , which coincides in the limit  $m_h^2/Q^2 \rightarrow 0$  with its zero-mass  $\overline{\text{MS}}$  expression in Eq. (8) of Ref. [20]. For the longitudinal function  $F_L$ , the heavy-quark subtraction  $A_{l,l,heavy}^{NS,(2)}$  is zero. Putting everything together, we obtain the final expression for the NNLO light-quark component,

$$F_l^{(2)} = e_l^2 \left\{ C_{l,l}^{NS,(2)} \otimes (\Phi_{l/p} + \Phi_{\bar{l}/p}) + c^{PS,(2)} \otimes \Sigma + c_{l,g}^{(2)} \otimes \Phi_{g/p} \right\}, \quad (39)$$

where the Wilson coefficients are listed in Eqs. (29)-(31) and (34)-(37).

#### D. Several heavy flavors, semi-inclusive heavy quark production

Structure functions  $F_l$  and  $F_h$  in Eqs. (39) and (24) are all that is needed to compute inclusive  $F(x, Q)$ . Our expressions can be also extended to include two or more heavy-quark flavors:

$$F = \sum_{l=1}^{N_l} F_l + \sum_{h=N_{l+1}}^{N_f^{fs}} F_h, \quad (40)$$

where the sum runs over all quark flavors satisfying  $4m_h^2 \leq W^2$  (*i.e.*, up to the total number  $N_f^{fs}$  of quark flavors which can be produced in pairs for the given energy  $W$ ).

A clarification is in order that the heavy-quark component  $F_h$  of inclusive  $F(x, Q)$  (defined as the part proportional to the heavy-quark electric charge  $e_h^2$ ) is not directly measurable. Rather, experiments publish the semi-inclusive (SI) heavy-quark structure function  $F_{h,SI}(x, Q)$  that is determined from the cross section with at least one registered heavy meson. In the case of  $F_2$  at NNLO,  $F_{h,SI}(x, Q)$  with  $h = c$  essentially coincides with the charm structure function  $F_2^{(c)}$  that is commonly measured by HERA experiments.

While  $F_{h,SI}$  must be defined with care to obtain infrared-safe results at all  $Q$  [13], for a global fit it is sufficient to approximate  $F_{h,SI}$  in the following way [18]. At moderate  $Q$  values accessible at HERA, we define it as

$$F_{h,SI}(x, Q) = F_h(x, Q) + \sum_{l=1}^{N_l} e_l^2 L_{I,q}^{NS,(2)} \otimes (\Phi_{l/p} + \Phi_{\bar{l}/p}). \quad (41)$$

Here  $F_h(x, Q)$  is the component with the heavy quark struck by the photon, cf. Eqs. (12) and (24).  $L_{I,q}^{NS,(2)}$  is the non-singlet part of the light-quark component  $F_l(x, Q)$  that contains radiation of a  $h\bar{h}$  pair in the final state, as shown in Fig. 2(a). This is the same function that

was discussed in the previous subsection, and it is computed explicitly in Ref. [40]. However, since the virtual diagram in Fig. 2(b) does not contribute to  $F_{h,SI}$ , the plus prescription is not imposed on  $L_{I,q}^{NS,(2)}$  in this case.

The  $F_{h,SI}(x, Q)$  function that is thus defined is numerically stable in comparisons to the existing data [18]. Our numerical analysis shows that the contribution associated with  $L_{I,q}^{NS,(2)}$  provides between 0 and 3% of the semi-inclusive charm cross sections at  $Q < 10$  GeV, which is insignificant compared to typical experimental errors.

### E. Factorization and $\chi$ convention

In the remainder of this section, we show that the S-ACOT- $\chi$  scheme is fully compatible with the QCD factorization theorem for DIS.

To see why the  $\chi$  convention is needed, consider again the heavy-quark contribution to  $F(x, Q)$  on the proton,

$$F_h(x, Q) = e_h^2 \sum_{l=1}^{N_l} \int_{\chi}^1 \frac{d\xi}{\xi} C_{h,l} \left( \xi p, m_h, \frac{Q}{\mu_0} \right) \Phi_{l/p}(\xi, \mu_0). \quad (42)$$

This expression is the same as in Eq. (12), but it assumes a low factorization scale  $\mu_0 \approx 1$  GeV, at which only PDFs for light parton flavors ( $l = 0, \dots, N_l$ ) are present. The convolution limits in Eq. (42) are such that the light parton  $l$  entering the coefficient function carries enough energy to produce one  $h\bar{h}$  pair or more in the final state. As  $\mu$  increases, a coefficient function  $C_{h,h}$  with an initial-state heavy quark is introduced at the switching point from  $N_l$  to  $N_{l+1}$  active flavors. This function does not automatically vanish outside of the physical range  $\chi \leq \xi \leq 1$ . If  $C_{h,h}$  is defined so as to contribute in a wider range  $\xi_{min} \leq \xi \leq 1$  at the switching point, with  $x \leq \xi_{min} < \chi$ , then the same wider range will be preserved at all  $\mu$  above the switching point by the DGLAP evolution.

If  $\widehat{W}$  is the center-of-mass energy of the photon scattering on a *light* parton  $a$ ,

$$\widehat{W}^2 \equiv (p_a + q)^2 = Q^2 (\xi/x - 1), \quad (43)$$

it must be larger than the  $h\bar{h}$  pair mass for *any*  $h\bar{h}$  production subprocess to occur:

$$4m_h^2 \leq \widehat{W}^2 \leq W^2 = Q^2(1/x - 1). \quad (44)$$

According to this condition, the scattering probability is non-zero only if the momentum fraction  $\xi$  is in the range

$$\chi \leq \xi \leq 1, \quad (45)$$

where  $\chi = x(1 + 4m_h^2/Q^2) \geq x$ .

If collinear approximations for flavor-excitation (FE) and subtraction terms in  $C_{h,a}$  violate this fundamental requirement, large spurious contributions from the unphysical kinematical region cancel to each order of  $\alpha_s$ , but survive as higher-order logarithmic terms. They can be eliminated by a supplemental condition that correct integration limits are always to be preserved, as in Eq. (45).<sup>3</sup>

---

<sup>3</sup> Even in the  $Q^2 \gg m_h^2$  limit, convolutions with FE terms and subtractions could be in principle extended

We will now show how to apply this condition at any order by including it into the QCD factorization theorem. For this purpose, we examine the projection operator  $Z$  that encapsulates the main rules of each factorization scheme [3]. It applies a set of approximations to Feynman graphs with leading momentum regions in order to enable all-order factorization.

Feynman graphs containing the leading DIS contributions are composed of two-particle irreducible subgraphs  $H$  and  $T$ , joined by one parton line on each side of the unitarity cut. Each leading graph  $H \cdot T$  involves integration over the momentum  $k^\mu$  of the intermediate parton and summation over its spin components,

$$H \cdot T \equiv \sum_{a=g,u,\bar{u},d,\bar{d},\dots} \int \frac{d^4 k}{(2\pi)^4} \sum_{spins} H_a(q, k) T_a(k, p). \quad (46)$$

Virtualities of all momenta are of order  $Q$  in the hard subgraph  $H_a(q, k)$ , and they are much smaller than  $Q$  in the target subgraph  $T_a(k, p)$ .  $q^\mu$  and  $p^\mu$  are the photon's and proton's 4-momenta. The nearly massless proton moves in the  $+z$  direction in the Breit reference frame.

The purpose of the  $Z$  operator is to approximate the leading-power (logarithmically divergent) part of  $H \cdot T$  by a simpler expression, denoted by  $H \cdot Z \cdot T$ , and to recast  $H \cdot T$  as

$$H \cdot T = \sum_a \int \frac{d^4 k}{(2\pi)^4} \int \frac{d^4 l}{(2\pi)^4} \sum_{spins} H_a(q, l) Z_a(l, k; \hat{l}) T_a(k, p) + \text{non-leading power term}. \quad (47)$$

The leading-power approximation  $H \cdot Z \cdot T$  provides the bulk of  $H \cdot T$ . The non-leading power part is suppressed by terms of order

$$\left( \frac{\text{highest virtuality in } T}{\text{lowest virtuality in } H} \right)^r, \text{ with } r > 0.$$

When it is recursively applied to all leading subgraphs, the  $Z$  projection generates the factorized expression for the structure function,  $F = \sum_a [C_a \otimes f_a] + \mathcal{O}(\Lambda_{QCD}/Q)$ . [3]

The  $Z$  operation simplifies integration over the momentum and summation of the spin of the intermediate parton, and it also simplifies the hard graph  $H$ . The momentum  $l^\mu$  of the parton  $a$  that enters  $H$  is replaced by a simpler momentum  $\hat{l}^\mu$ , *e.g.*,  $\hat{l}^\mu = \xi p^\mu$  if  $a$  is massless. The  $Z$  operation discards suppressed terms in  $H$ , notably, masses of the light quarks, and specifies how to handle the heavy-quark masses in  $H$ .

Variants of the ACOT scheme are distinguished by the form of the operator  $Z_h$  that acts on the  $H$  subgraphs with an incoming heavy-quark line. The target parts  $T_a$ , and the operators  $Z_l$  and  $Z_g$  for the  $H$  subgraphs with initial light-quark and gluon lines are the same in all variants. The PDFs in  $T_a$  are defined by operator matrix elements as in Eq. (3) and retain mass dependence.

The  $Z_h$  operator is of the form

$$Z_h(l, k; \hat{l}) = \frac{1}{4} (2\pi)^4 S_H(\hat{l}) S_T \delta(l^+ - \hat{l}^+) \delta(l^- - \hat{l}^-) \delta^2(\vec{l}_T),$$

---

to include contributions from  $0 \leq \xi \leq x$ . This would not violate QCD factorization order by order, but destabilize higher-order terms. This is avoided by an implicit assumption that the FE convolutions in the ZM limit are restricted to the physical range  $x \leq \xi \leq 1$ .

Scheme	$\widehat{l}^\mu$ in $Z_h$	$S_H$	$m_h$ in $H_h(q, \widehat{l})$	$\xi$ range in $H_h \cdot T_h$
ACOT	$(\xi p^+, \frac{m_h^2}{2\xi p^+}, \vec{0}_T)$	$\frac{\widehat{l} \cdot \gamma + m_h}{\xi p^+}$	$m_h \neq 0$	$\frac{x}{2} \left(1 + \sqrt{1 + \frac{4m_h^2}{Q^2}}\right) \leq \xi \leq 1$
S-ACOT	$(\xi p^+, 0, \vec{0}_T)$	$\gamma^-$	$m_h = 0$	$x \leq \xi \leq 1$
S-ACOT- $\chi$	$(\xi \frac{p^+}{1+4m_h^2/Q^2}, 0, \vec{0}_T)$	$\gamma^-$	$m_h = 0$	$x (1 + 4m_h^2/Q^2) \leq \xi \leq 1$

TABLE I: Components of the projection operator  $Z_h(l, k; \widehat{l})$  in three versions of the ACOT scheme.

where  $S_H(\widehat{l})$  and  $S_T = \gamma^+$  are projectors on the leading spin components in  $H$  and  $T$ , respectively. The incoming heavy quark in  $H_h$  has an approximate momentum  $\widehat{l}^\mu$ , where the light-cone components of  $\widehat{l}^\mu$  in the Breit frame are  $\widehat{l}^\pm \equiv (\widehat{l}^0 \pm \widehat{l}^3)/\sqrt{2}$  and  $\vec{l}_T = 0$ . With this representation, the  $H_h \cdot Z_h \cdot T_h$  integral assumes the form of a convolution over  $\xi$ ,

$$H_h \cdot Z_h \cdot T_h = \int \frac{d\xi}{\xi} \text{tr} \left[ H_h(q, \widehat{l}) \frac{S_H(\widehat{l})}{2} \right] \int \frac{dk^- d^2 \vec{k}_T}{(2\pi)^4} \text{tr} \left[ \frac{\gamma^+}{2} T_h(k, p) \right], \quad (48)$$

where  $\xi = \widehat{l}^+/p^+$  is the ratio of large “+” momentum components.

Table I collects expressions for  $\widehat{l}^\mu$  and  $S_H(\widehat{l})$  in the ACOT, S-ACOT, and S-ACOT- $\chi$  schemes. It also specifies integration ranges in the  $H_h \cdot T_h$  convolutions and indicates if  $m_h$  is set to zero in the  $H_h$  subgraphs. We re-emphasize that the three schemes differ only in the Wilson coefficients with initial-state heavy quarks, *i.e.*, in the flavor-excitation channel.

In Table I, we observe that the schemes differ by moderate terms in  $H_h(q, l)$  that are proportional to powers of  $m_h^2/Q^2$ . The form of these terms is not specified by the factorization theorem. It is allowed to simplify the FE hard-scattering contributions by setting  $m_h = 0$  as in the S-ACOT scheme. In the full ACOT scheme, the lower limit of integration in  $H_h \cdot Z_h \cdot T_h$  is set by the kinematics of scattering of a massive quark into a massive quark, which violates the momentum conservation condition of Eq. (42) for pair production of massive quarks from light-quark scattering. In the S-ACOT scheme, one is tempted to set the integration range to  $x \leq \xi \leq 1$ , which is also incompatible with momentum conservation. One cannot just restrict the integration range to  $\chi \leq \xi \leq 1$ , as this disallows the lowest-order FE contribution  $c_{h,h}^{(0)} \otimes h$  that contributes at  $\xi = x$ .

A better way is provided by rescaling  $\xi \rightarrow \widetilde{\xi} = \kappa \xi$ ,  $p^+ \rightarrow \widetilde{p}^+ = p^+/\kappa$ , which leaves  $H(q, \widehat{l})$  invariant, as it does not change  $\widehat{l}^\mu$ ,  $\widehat{x} = Q^2/(2\widehat{l} \cdot q)$ , or other kinematical variables in  $H(q, \widehat{l})$ . At the same time, rescaling changes the integration range for  $\xi$  in the convolution.

Choosing  $\kappa = (1 + 4m_h^2/Q^2)$ , we obtain the S-ACOT- $\chi$  scheme that has all desirable features:

1. The proof of QCD factorization for the S-ACOT scheme in [3] also applies to the S-ACOT- $\chi$  scheme, since the S-ACOT and S-ACOT- $\chi$  schemes have the same  $H(q, \widehat{l})$ . The  $Z$  operation of the S-ACOT- $\chi$  scheme upholds all expected properties that are listed in Sec. 9C of [3].
2. The integration over  $\xi$  proceeds over the physical range  $\chi \leq \xi \leq 1$  in all channels. It



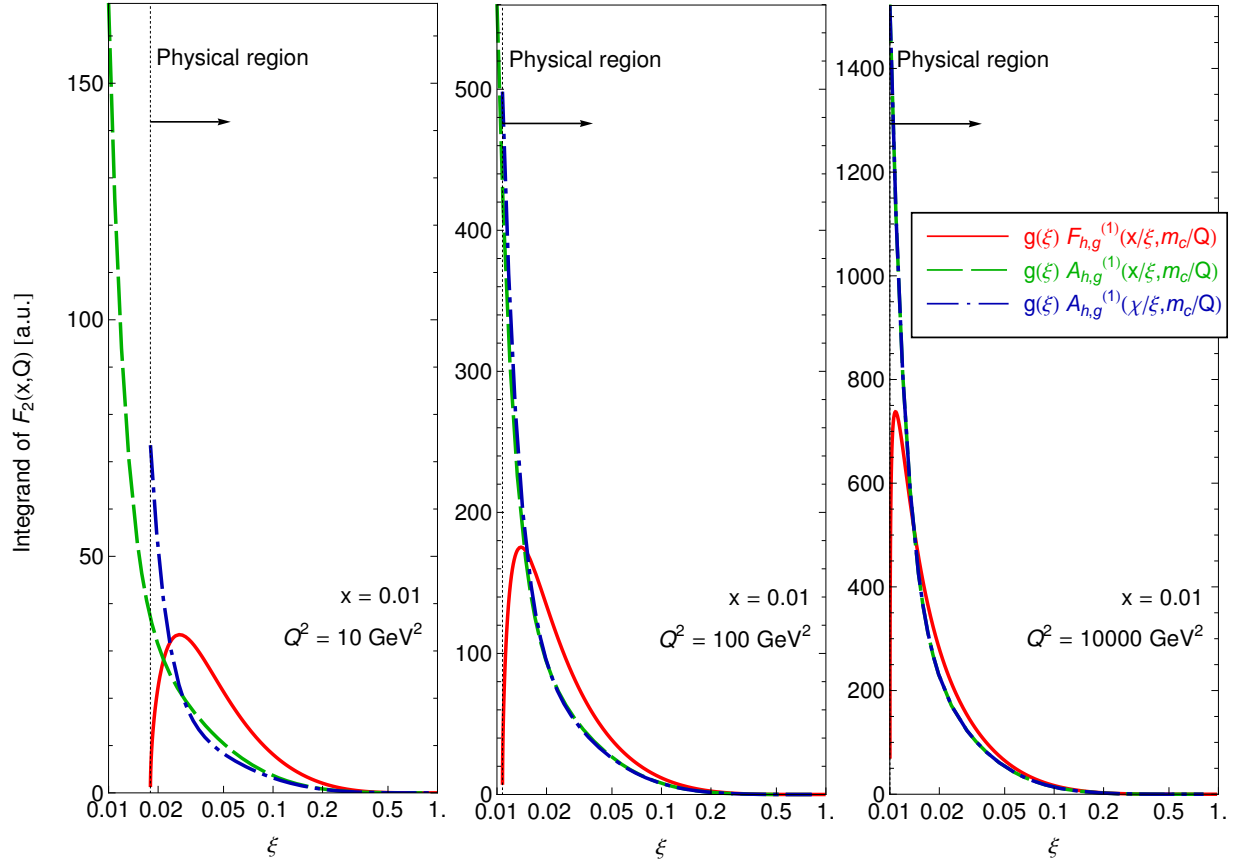


FIG. 3: Integrands of convolution integrals  $F_{h,g}^{(1)} \otimes g$  and  $A_{h,g}^{(1)} \otimes g$  with and without the  $\chi$  prescription, plotted as a function of the momentum fraction  $\xi$ .

includes all physically possible scattering channels, but excludes kinematically prohibited  $\xi$  values.

3. The S-ACOT- $\chi$  coefficient functions  $H_h$  in the flavor-excitation channels are given by ZM expressions evaluated at  $\hat{x} = \chi/\xi$ . Kinematical prefactors in front of the coefficient functions that are independent of  $\xi$  are not modified.
4. The target subgraphs  $T_a$ , corresponding to the PDFs, are given by universal operator matrix elements that are the same in all ACOT-like schemes.
5. When  $Q$  is much larger than  $m_h$ , the S-ACOT- $\chi$  scheme reduces to the zero-mass  $\overline{\text{MS}}$  scheme, without additional finite renormalizations.
6. When  $Q$  is of order  $m_h$ , the S-ACOT- $\chi$  scheme approaches the FFN scheme faster than the S-ACOT scheme. Better matching on the FFN scheme is a consequence of the  $Z$  operation that satisfies energy conservation. It does not rely on propositions beyond the factorization theorem with energy conservation, such as conditions for derivatives of  $F(x, Q)$  [15] or damping factors [18].

*An illustration for the  $\chi$  convention*

The advantages of  $\chi$  rescaling can be demonstrated on the example of the  $\mathcal{O}(\alpha_s)$   $\gamma^*g$  contribution, consisting of the gluon-initiated box graph and corresponding subtraction, and shown by the second and third graphs on the upper row of Fig. 1:

$$[C_{h,g}^{(1)} \otimes g](x, Q) = \int_{\chi}^1 \frac{d\xi}{\xi} g(\xi, Q) F_{h,g}^{(1)}\left(\frac{\chi}{\xi}\right) - \int_{\zeta}^1 \frac{d\xi}{\xi} g(\xi, Q) A_{h,g}^{(1)}\left(\frac{\zeta}{\xi}\right). \quad (49)$$

The integrands of the convolution integrals on the right-hand side,  $g(\xi, Q) F_{h,g}^{(1)}(\chi/\xi)$  and  $g(\xi, Q) A_{h,g}^{(1)}(\zeta/\xi)$ , where  $\zeta = x$  or  $\chi$ , are plotted in Fig. 3(a-c) as a function of  $\xi$ . The computation follows the numerical setup described in the next section. The scale on the  $\xi$  axis is logarithmic: the convolution integrals are proportional to areas under respective integrand curves. For definiteness, we choose  $x = 0.01$  and  $Q^2 = 10, 100$ , and  $10000 \text{ GeV}^2$ , but the same features are observed for other  $x$  and  $Q$  values.

In the charm creation contribution,  $g \otimes F_{hg}^{(1)}$ , the integrand (red solid line) vanishes outside of the physical range  $\chi \leq \xi \leq 1$ , where  $\chi \approx 0.018, 0.0108$ , and  $0.010008$  for  $Q^2 = 10, 100$ , and  $10000 \text{ GeV}^2$ . On the other hand, the naive choice  $\zeta = x$  of the S-ACOT scheme allows the  $g(\xi, Q) A_{h,g}^{(1)}(\zeta/\xi)$  integrand (green dashed curve) to contribute in the unphysical region  $x \leq \zeta \leq \chi$ . Its spurious contribution is comparatively large at the smallest  $Q$ . It is not fully canceled by the counterpart FE term  $[c_{h,h}^{(0)} \otimes c](x, Q)$  in the first upper graph of Fig. 1, leading to a bloated higher-order uncertainty.

The S-ACOT- $\chi$  integrand  $g(\xi, Q) A_{h,g}^{(1)}(\chi/\xi)$  vanishes below  $\xi = \chi$  (cf. the blue dash-dotted line). It is numerically moderate at physical  $\xi$  values,  $\xi > \chi$ , and its integral cancels well with  $[c_{h,h}^{(0)} \otimes c](x, Q)$ , as will be further demonstrated in Sec. IV A. Note also that the difference between the two definitions for the  $g(\xi, Q) A_{h,g}^{(1)}(\zeta/\xi)$  integrand is small in most of the physical range  $\chi \leq \xi \leq 1$ .

As the virtuality  $Q$  increases, the difference between  $\chi$  and  $x$  progressively reduces, letting  $\xi$  to vary in a larger interval. Finally in (c), for very large  $Q$ , the S-ACOT and S-ACOT- $\chi$  subtractions become identical.  $A_{h,g}^{(1)} \otimes g$  approximates well the collinear splitting contribution that drives much of the shape of  $F_{h,g}^{(1)}(\chi/\xi)g(\xi)$ . When  $A_{h,g}^{(1)} \otimes g$  is subtracted from  $F_{h,g}^{(1)} \otimes g$  as in Eq. (49), it produces a moderate *negative*  $\mathcal{O}(\alpha_s)$  contribution, which is further reduced at NNLO. These cancellations are further examined in Sec. IV B.

### III. NUMERICAL EXAMPLES

In this section, we show representative plots from our validation tests for NNLO inclusive structure functions  $F_2(x, Q)$  and  $F_L(x, Q)$  computed according to the S-ACOT- $\chi$  method. We focus on partial contributions in which the photon strikes a charm quark, given by  $F_h(x, Q)$  in Eq. (12) for  $h = c$ , and for structure functions  $F = F_2$  or  $F_L$ . These contributions are referred to as  $F_{2c}(x, Q)$  and  $F_{Lc}(x, Q)$  in the figures. The same comparisons have been repeated for bottom-quark functions  $F_{2b}$  and  $F_{Lb}$ , as well as for the full inclusive functions  $F = \sum_{l=1}^{N_l} F_l + \sum_{h=N_l+1}^{N_f^{fs}} F_h$  and alternative values of Bjorken  $x$ . The results of other tests show similar patterns and can be viewed at [45].

NNLO heavy-quark coefficient functions are computed using a program available from [27]. This program tabulates two-loop heavy-quark coefficient functions in a form that allows fast evaluation of convolution integrals in the  $Q$  range covered by the experimental data.

The PDFs in all comparisons are obtained by using the Les Houches Accord toy parametrization [46, 47] at the starting scale  $Q_0 = m_c = \sqrt{2}$  GeV. Other input parameters are  $\alpha_s(Q_0) = 0.36$  and the pole mass  $m_c$ .<sup>4</sup> The switching between 3 and 4 flavors happens at  $Q = m_c$ . The  $\alpha_s$  and PDFs are evolved to higher  $Q$  values by the HOPPET computer code [48].<sup>5</sup>

#### A. $Q$ dependence

Fig. 4 examines  $Q$  dependence of charm structure functions  $F_{2c}$  (left panel) and  $F_{Lc}$  (right panel). They are computed to order  $\alpha_s^2$  in all schemes, referred to as “NNLO” by the counting convention adopted here. The upper insets in both panels show predictions at  $x = 10^{-2}$  in the S-ACOT- $\chi$  scheme, FFN scheme with  $N_f = 3$ , and ZM scheme with  $N_f = 4$ . The lower insets show ratios of the FFN and ZM predictions to the S-ACOT- $\chi$  prediction.

The left panel shows that the S-ACOT- $\chi$  theory prediction for  $F_{2c}(x, Q)$  (blue solid line) is numerically close to the FFN prediction (red short-dashed line) at  $Q \approx m_c$  and to the ZM prediction (magenta long-dashed line) at  $Q > 10$  GeV.

Similarly, in the right panel, the S-ACOT- $\chi$  prediction for the longitudinal function  $F_{Lc}(x, Q)$  coincides with the corresponding FFN prediction at  $Q \approx m_c$  and approaches the

<sup>4</sup> Our program can alternatively read  $\overline{\text{MS}}$  masses as the input. In this case, the  $\overline{\text{MS}}$  masses are later converted into pole masses, because the operator matrix elements  $A_{ab}^{(k)}$  are published as functions of the pole mass.

<sup>5</sup> Bottom-quark contributions are omitted in this comparison. The charm PDF is zero at  $Q < Q_0 = m_c$ , but acquires a non-negligible value immediately above  $Q_0$  through an  $\mathcal{O}(\alpha_s^2)$  discontinuity existing at the switching point.

ZM prediction at  $Q > 30$  GeV. [ $F_{Lc}(x, Q)$  is sensitive to mass-dependent corrections to scattering off longitudinally polarized photons. Its matching on the ZM prediction happens at higher  $Q$  values than in  $F_{2c}$ .] The S-ACOT- $\chi$  prediction interpolates between the FFN and ZM predictions at intermediate  $Q$  values, precisely as expected.

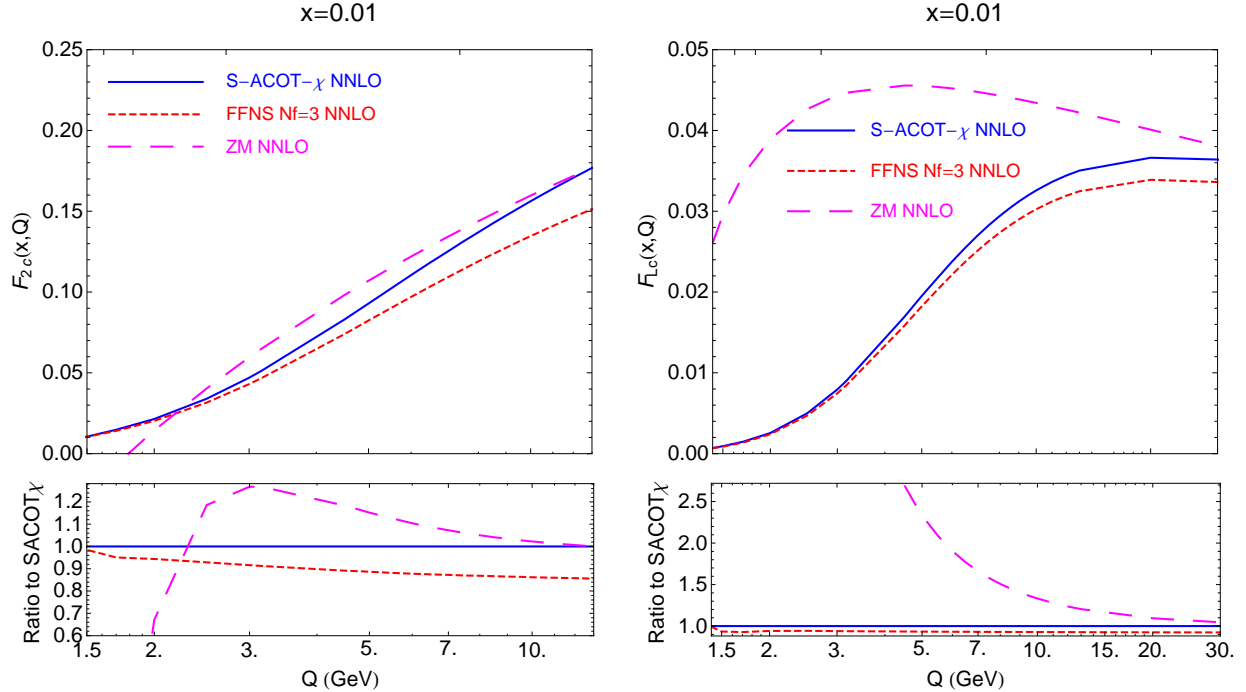


FIG. 4: Comparison of  $F_{2c}(x, Q)$  (left) and  $F_{Lc}(x, Q)$  computed at  $\mathcal{O}(\alpha_s^2)$  in the S-ACOT- $\chi$  (solid), FFN  $N_f = 3$  (short dashed), and ZM  $N_f = 4$  (long dashed) schemes, shown as a function of  $Q$  at  $x = 10^{-2}$ .

## B. Dependence on the factorization scale

NLO computations leave substantial uncertainty in DIS charm-quark contributions due to the choice of the renormalization/factorization scale and differences in FE terms in the threshold region. NNLO terms drastically reduce these uncertainties. Factorization scale dependence, and its reduction from NLO to NNLO, is illustrated by Fig. 5. Reduction in uncertainties in the modeling of kinematical threshold effects is discussed in Sec. III E.

In Fig. 5(a)-(c), predictions for  $F_{2c}(x, Q)$  in the S-ACOT- $\chi$  and FFN ( $N_f = 3$ ) schemes are plotted versus Bjorken  $x$  at representative  $Q^2$  values of 4, 10, and 100 GeV<sup>2</sup>. The  $F_{2c}(x, Q)$  values on the  $y$  axis are multiplied by  $10^3\sqrt{x}$  to better visualize the accessible  $x$  region. Central predictions are computed for  $\mu = \sqrt{Q^2 + m_c^2}$ , the default scale in heavy-quark DIS cross sections in the CT10 global analysis [6]. The error bands are obtained by varying the scale in the range  $Q \leq \mu \leq \sqrt{Q^2 + 4m_c^2}$ .

At  $Q = 2$  GeV in Fig. 5(a), the NNLO S-ACOT- $\chi$  central prediction (black solid line inside a green band) is slightly above the NNLO FFN prediction (short-dashed line inside a magenta band) and has smaller scale uncertainty than FFN. At  $Q$  below 2 GeV (not shown), the NNLO S-ACOT- $\chi$  and FFN predictions get even closer. In contrast, the NLO S-ACOT-

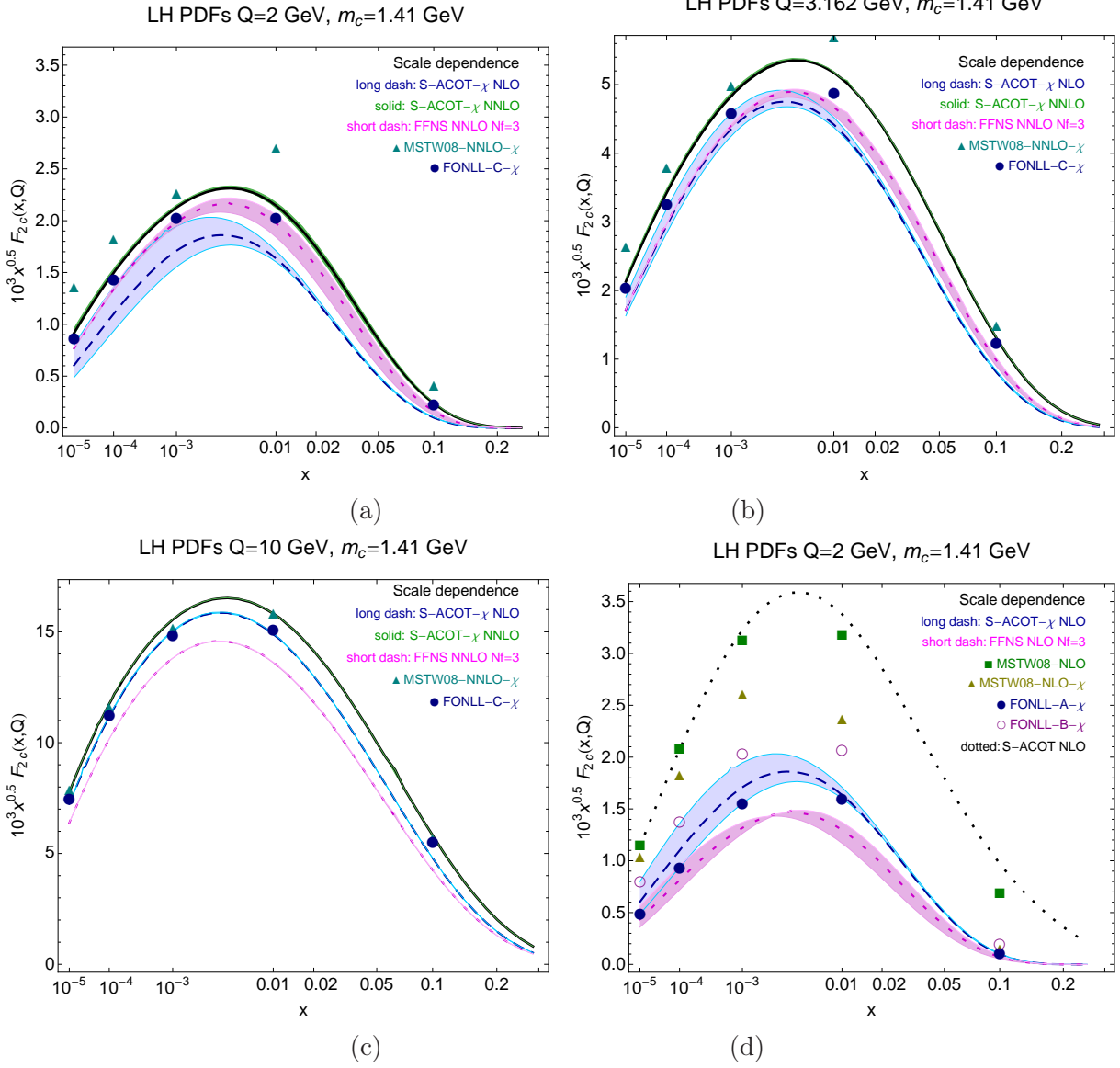


FIG. 5: Comparison of predictions for  $F_{2c}(x, Q)$  in the S-ACOT- $\chi$  scheme and alternative theoretical approaches at NLO and NNLO. Central predictions are for  $\mu = \sqrt{Q^2 + m_c^2}$ , and the error bands are for  $Q \leq \mu \leq \sqrt{Q^2 + 4m_c^2}$ .

$\chi$  prediction (a long-dashed line inside a blue band) underestimates the NNLO FFN result and has wider scale dependence.

As  $Q$  increases to 10 GeV (Fig. 5(c)), S-ACOT- $\chi$  predicts more event rate than the FFN scheme both at NLO and NNLO. Altogether, the  $Q$  dependence in these figures is fully compatible with the matching of the S-ACOT- $\chi$  results on the FFN and ZM results in the limits  $Q^2 \approx m_c^2$  and  $Q^2 \gg m_c^2$ , respectively.

### C. Alternative factorization schemes

Figs. 5(a)-(c) also show NNLO predictions in alternative GM schemes, indicated by scattered symbols: the modified Thorne-Roberts (TR') scheme [14–16] as implemented by the MSTW'08 PDF analysis [49]; and FONLL scheme C used by the NNPDF collaboration [18]. Their values are computed in the 2009 Les Houches benchmark study of GM schemes [50] by assuming the same  $\chi$  rescaling as the S-ACOT- $\chi$  scheme.

The three schemes are seen to be in good overall agreement, apart from minor differences traced to subtle variations in the NNLO implementations that the schemes provide.

At  $Q = 2$  GeV, the NNLO S-ACOT- $\chi$  prediction lies slightly above the FONLL-C prediction and below the MSTW prediction. At  $Q = 10$  GeV, the NNLO S-ACOT- $\chi$  prediction becomes closer to the MSTW prediction and is still above the FONLL-C result. These differences can be understood by noticing that the compared schemes may differ in subleading perturbative terms. For example, the FONLL-C scheme includes a threshold damping factor to match on the 3-flavor result near the threshold [18]. The S-ACOT- $\chi$  scheme is not using the damping factor and is expectedly close to the FONLL-C scheme at  $Q \rightarrow m_c$ , but not strictly identical. The TR'/MSTW prediction includes a constant higher-order term (of order  $\mathcal{O}(\alpha_s^3)$ ) to improve smoothness of switching from 3 to 4 flavors at  $Q = m_c$ . Neither S-ACOT- $\chi$  nor FONLL-C includes such term, which is why they may predict smaller  $F_{2c}$  values at low  $Q$ .

### D. NNLO vs. NLO predictions

Improved stability of the NNLO prediction in Fig. 5(a) can be appreciated by comparing it to the counterpart NLO result shown in Fig. 5(d). Here, we collect a variety of NLO  $F_{2c}(x, Q)$  values at  $Q = 2$  GeV, obtained in FFN, S-ACOT, TR'/MSTW, FONLL-A, and FONLL-B schemes. The S-ACOT and MSTW predictions are shown with the  $\chi$  scaling as well as without it.

The spread in NLO values of  $F_{2c}(x, Q)$  observed in the figure is extensive, nominally suggesting a large uncertainty in the resulting NLO PDF sets. However, when included in the PDF fits, the most extreme predictions for  $F_{2c}(x, Q)$  in this figure are excluded by the fitted DIS data, which prefer the values that are about the same as the (relatively unambiguous) NNLO result. In CT10 fit, the scale  $\mu$  is set equal to  $\sqrt{Q^2 + m_c^2}$ , which brings the NLO S-ACOT- $\chi$  prediction in agreement with the measured cross sections. Thus, according to the past global fits, the NLO cross sections can be reconciled with the heavy-quark data, but at the expense of tuning of the scale parameter, for each value of  $m_c$  and rescaling variable. The key benefit of the NNLO calculation for  $F_{2c}(x, Q)$  is to automatically achieve such a good agreement, nearly independently of the factorization scale.



### E. Threshold effects

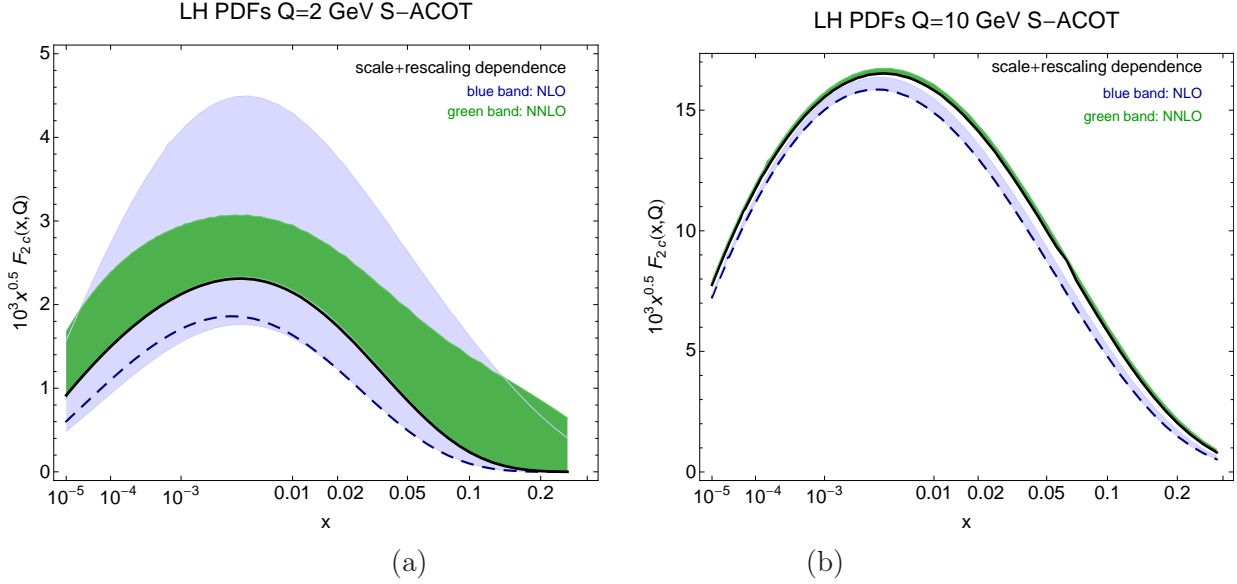


FIG. 6: Dependence on the factorization scale  $\mu$  and the rescaling variable  $\zeta(\lambda)$ . Left:  $Q = 2$  GeV; right:  $Q = 10$  GeV.

In the above discussion, our NNLO structure functions are computed using the optimal rescaling variable  $\zeta = \chi$  in the FE heavy-quark contributions. The rescaling variable significantly improves convergence near the threshold, by excluding contributions to the FE convolution integrals that are kinematically impossible.

Dependence on the rescaling variable can be explored with the help of a generalization of the  $\chi$  variable proposed in Ref. [33] and designated by  $\zeta$ . The generalized rescaling variable  $\zeta$  is implicitly defined by

$$x = \frac{\zeta}{1 + \zeta^\lambda \cdot (4m_c^2)/Q^2}, \quad (50)$$

where  $\lambda$  is a real number. Various choices of positive  $\lambda$  produce a family of GM schemes in which  $\zeta$  takes continuous values between  $x$  (no rescaling) and  $\chi$  (full rescaling). Specifically,  $\lambda = 0$  produces  $\zeta = \chi$  of the S-ACOT- $\chi$  scheme, and  $\lambda \gg 1$  produces  $\zeta \approx x$  that corresponds to the plain S-ACOT scheme without rescaling. Negative  $\lambda$  values (not shown) strongly suppress the FE contributions by setting  $\zeta > \chi$ .

Fig. 6 shows the bands of variations in the NLO and NNLO S-ACOT  $F_{2c}$  values at  $Q = 2$  GeV (left panel) and 10 GeV (right panel) when  $\mu$  and  $\lambda$  are varied in the ranges  $Q \leq \mu \leq \sqrt{Q^2 + 4m_c^2}$  and  $0 \leq \lambda \leq 100$ , respectively. If  $\lambda$  is naively varied in the full range, at smallest  $Q$  values one obtains a large excursion in NLO predictions (light blue band), which is considerably reduced when going to NNLO (green band). As  $Q$  increases above a few GeV, dependence on  $\lambda$  diminishes practically to nil, as in the right panel of the figure for  $Q = 10$  GeV. Together with Fig. 5, Fig. 6 indicates that the physically motivated rescaling variable is more important at low  $Q$  and NNLO than the factorization scale choice.

## IV. CANCELLATIONS BETWEEN FEYNMAN GRAPHS

### A. Cancellations at low $Q$

In order to match on the FFN and ZM predictions, certain classes of Feynman diagrams inside the S-ACOT- $\chi$  NNLO coefficient functions must cancel in the respective low- $Q$  and large- $Q$  regions. We will show how these cancellations come about in the case of the charm-quark function  $F_{2c}(x, Q)$ , but the pattern holds for the bottom quark and other structure functions with suitable modifications.

The cancellations are revealed by plotting differences between various matrix elements and collinear subtractions discussed in Section II A, which are established by applying the factorization formula at the parton level.

In the  $Q \approx m_c$  region, all FE contributions in Eqs. (18)-(21) must cancel to a high degree, in order for  $F_{2c}(x, Q)$  to reduce to the FFN matrix elements  $F_{h,g}^{(1,2)}$  and  $F_{h,l}^{(2)}$ . In the threshold region, the evolved charm PDF is effectively of order  $\mathcal{O}(a_s)$ ,

$$\lim_{Q^2 \rightarrow m_c^2} c(x, Q) \approx a_s(Q) \left[ A_{hg}^{(1)} \otimes g \right] (x, Q); \quad (51)$$

a FE contribution to  $F_{2c}(x, Q)$  containing a coefficient  $c_{h,h}^{(k)}$  is effectively of order  $\mathcal{O}(a_s^{k+1})$ . Keeping this in mind, at order  $\mathcal{O}(\alpha_s)$  the virtual-photon-charm scattering diagram with  $c_{h,h}^{(0)}$  in Eq. (18) cancels the gluon-initiated subtraction term with  $A_{hg}^{(1)}$  in Eq. (19), and only the  $\gamma^*g$  fusion diagram  $F_{hg}^{(1)}$  in Eq. (19) survives in the total  $F_{2c}(x, Q)$ . In this case, the difference

$$D_{C(0)}^{(1)}(x, Q) = \left[ c_{h,h}^{(0)} \otimes c \right] (x, Q) - a_s \left[ c_{h,h}^{(0)} \otimes A_{hg}^{(1)} \otimes g \right] (x, Q), \quad (52)$$

where  $c(x, Q)$  and  $g(x, Q)$  represent the charm and gluon PDFs, must be close to zero.

As the next order is included, the cancellation present in  $D_{C(0)}^{(1)}$  must further improve. Two differences quantify the cancellations to this order:

$$D_{C(0)}^{(2)}(x, Q) = D_{C(0)}^{(1)}(x, Q) - a_s^2 \left[ c_{h,h}^{(0)} \otimes A_{hg}^{(2)} \otimes g \right] (x, Q) - a_s^2 \left[ c_{h,h}^{(0)} \otimes A_{hl}^{PS,(2)} \otimes \Sigma \right] (x, Q), \quad (53)$$

in which the convolutions of  $c_{h,h}^{(0)}$  with  $\mathcal{O}(\alpha_s^2)$  operator matrix elements  $A_{hg}^{(2)}$  and  $A_{hl}^{PS,(2)}$  are subtracted from  $D_{C(0)}^{(1)}(x, Q)$ ; and

$$D_{C(1)}^{(2)}(x, Q) = a_s \left[ c_{h,h}^{(1)} \otimes c \right] (x, Q) - a_s^2 \left[ c_{h,h}^{(1)} \otimes A_{hg}^{(1)} \otimes g \right] (x, Q), \quad (54)$$

which probes the cancellation between convolutions involving the coefficient  $c_{h,h}^{(1)}$ . By plotting the difference  $D_{C(0)}^{(2)}$ , we quantify how the  $\mathcal{O}(a_s)$  cancellation in  $D_{C(0)}^{(1)}$ , proportional to  $c_{h,h}^{(0)}$ , improves upon inclusion of the NNLO corrections. The difference  $D_{C(1)}^{(2)}$  quantifies an independent  $\mathcal{O}(a_s^2)$  cancellation, of the same structure as  $D_{C(0)}^{(1)}$ , but composed of the convolutions with  $c_{h,h}^{(1)}$  instead of  $c_{h,h}^{(0)}$ .

The left panel of Fig. 7 shows  $x$  dependence of  $D_{C(0)}^{(1)}$ ,  $D_{C(0)}^{(2)}$ , and  $D_{C(1)}^{(2)}$  at  $Q = 2$  GeV. To provide visual guidance, these differences are compared to the FFN  $N_f = 3$  prediction at

$\mathcal{O}(\alpha_s^2)$  (solid black line), which is roughly equal to the total rate at this  $Q$  (cf. the previous subsection). We also plot the S-ACOT- $\chi$  contribution of  $\mathcal{O}(\alpha_s^0)$  provided by  $c_{h,h}^{(0)}$  (dashed blue line), nominally counted as the lowest-order contribution. While the LO contribution on its own is substantial comparatively to the FFN result, it is mostly canceled by the subtraction in Eq. (52), so that the resulting difference  $D_{C^{(0)}}^{(1)}$  (long-dashed green line) is small.

The cancellation in  $D_{C^{(0)}}^{(1)}$  is further improved by including the next-order terms in  $D_{C^{(0)}}^{(2)}$  as in Eq. (53). The difference  $D_{C^{(0)}}^{(2)}$  (dot-dashed red line) and especially the counterpart difference  $D_{C^{(1)}}^{(2)}$  (dotted purple line) give decreasingly small contributions. They satisfy

$$\left| D_{C^{(1)}}^{(2)} \right| \ll \left| D_{C^{(0)}}^{(2)} \right| \ll \left| D_{C^{(0)}}^{(1)} \right| \leq F_{2,c}(x, Q). \quad (55)$$

Therefore, as  $Q \rightarrow m_c$ , the S-ACOT- $\chi$  scheme exhibits an almost perfect match on the FFN computation by virtue of perturbative cancellations that improve with each order of  $\alpha_s$ .

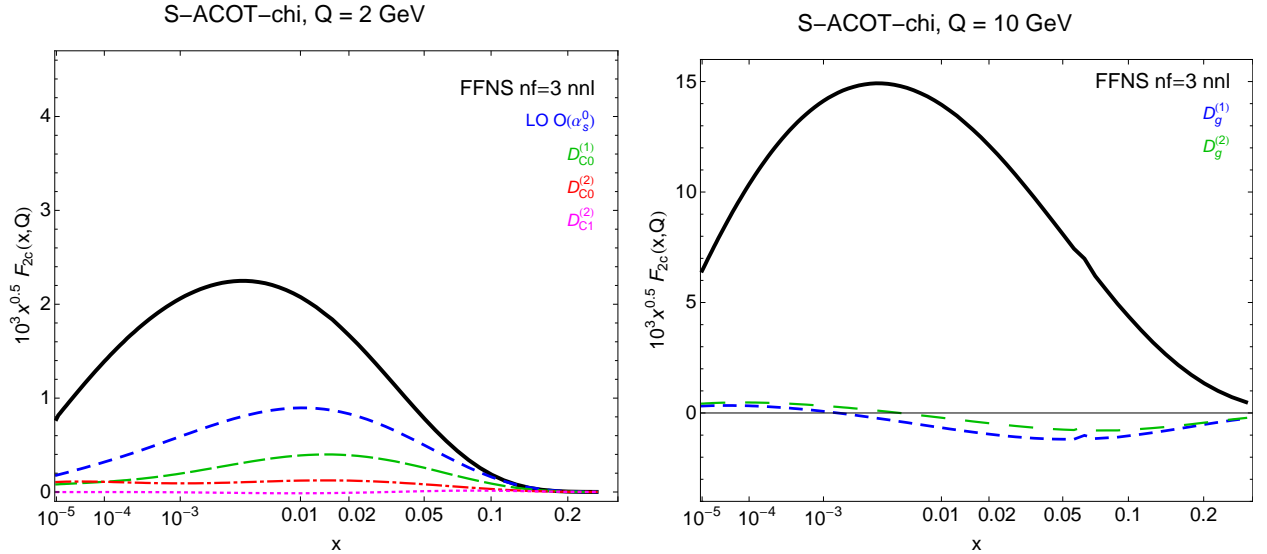


FIG. 7: Cancellations in the S-ACOT- $\chi$  scheme at  $Q^2 \approx m_c^2$  (left) and  $Q^2 \gg m_c^2$  (right).

## B. Cancellations at large $Q$

A different cancellation pattern is observed when  $m_c$  is negligible with respect to  $Q$ , when large logarithms collected in  $A_{hg}^{(1)}$ , etc. must be subtracted from massive contributions  $F^{(k)}$  to obtain infrared-safe  $C^{(k)}$ . These cancellations are illustrated in the right panel of Fig. 7 by  $D_g^{(1)}$  and  $D_g^{(2)}$  quantifying collinear subtractions in contributions containing the  $\gamma^*g$  box subgraph. The lowest-order difference  $D_g^{(1)}$  is equal to the convolution of the coefficient  $C_{h,g}^{(1)}$  as defined in Eq.(19):

$$D_g^{(1)}(x, Q) \equiv \left[ C_{h,g}^{(1)} \otimes g \right] (x, Q) = a_s \left\{ \left[ F_{h,g}^{(1)} \otimes g \right] (x, Q) - \left[ c_{h,h}^{(0)} \otimes A_{hg}^{(1)} \otimes g \right] (x, Q) \right\}. \quad (56)$$

In this expression the subtraction term matches on the  $\mathcal{O}(\alpha_s)$  photon-gluon contribution represented by  $F_{h,g}^{(1)}$ . The  $x$  dependence of this matching is shown in the right panel of Fig. 7 for  $Q = 10$  GeV. It can be seen that  $D_g^{(1)}$  (blue short-dashed line) is quite small compared to the  $\mathcal{O}(\alpha_s^2)$  FFN result.

The  $\alpha_s^2$ -order difference can be constructed as

$$D_g^{(2)}(x, Q) = D_g^{(1)}(x, Q) + a_s^2 \left\{ \left[ C_{h,g}^{(2)} \otimes g \right] (x, Q) + \left[ C_{h,l}^{(2)} \otimes \Sigma \right] (x, Q) \right\},$$

which can be cast into the form

$$\begin{aligned} D_g^{(2)} = D_g^{(1)} + a_s^2 \bigg\{ & \widehat{F}_{h,g}^{(2)} \otimes g + \widehat{F}_{h,l}^{PS,(2)} \otimes \Sigma - c_{h,h}^{(1)} \otimes A_{hg}^{(1)} \otimes g \\ & - c_{h,h}^{(0)} \otimes A_{hg}^{(2)} \otimes g - c_{h,h}^{(0)} \otimes A_{hl}^{PS,(2)} \otimes \Sigma \bigg\} \end{aligned} \quad (57)$$

by virtue of Eqs. (20) and (21). At this order, the collinear logarithms arising in  $\widehat{F}_{h,g}^{(2)}$  are canceled by  $c_{h,h}^{(0)} \otimes A_{hg}^{(2)}$  and  $c_{h,h}^{(1)} \otimes A_{hg}^{(1)}$ , and, similarly, the collinear term in  $\widehat{F}_{h,l}^{PS,(2)}$  is removed by  $c_{h,h}^{(0)} \otimes A_{hl}^{PS,(2)}$ . The net effect of the subtractions is that  $D_g^{(2)}$  (the green long-dashed line) provides a small correction to  $D_g^{(1)}$ . The perturbative series converge well for  $D_g^{(k)}$ :

$$|D_g^{(2)} - D_g^{(1)}| \ll |D_g^{(1)}| \ll F_2^c(x, Q). \quad (58)$$

### C. Cancellations without kinematic rescaling

Although the cancellations happen for any rescaling variable  $\zeta$ , their perturbative convergence is slower for a non-optimal choice, such as  $\zeta = x$ . The differences  $D_{C^{(0)}}^{(1)}$ , etc. for  $\zeta = x$  are shown in Fig. 8 and, as one can see, they are generally larger than in the case of  $\zeta = \chi$ . Nonetheless, the differences are reduced by going to NNLO, although not as fast as for the optimal rescaling choice.

## V. CONCLUSIONS

We examined connections between multi-loop calculations for massive quark production and fundamental concepts behind QCD factorization. An NNLO calculation for neutral-current DIS with massive quarks was documented in a form that bears structural similarity to the NNLO computation in the zero-mass scheme [19–21]. This calculation is algorithmic and utilizes readily available NNLO expressions. The main formulas are presented by Eqs. (40), (24), and (39).

The conceptual foundation for the presented results is provided by the S-ACOT- $\chi$  factorization scheme. The discussion emphasized several strong features of this scheme: its direct origin from the proof of QCD factorization for DIS [3], relative simplicity, and compliance with phase space constraints on heavy-quark production at all energies.

Throughout this study, we highlighted phenomenological importance of energy conservation in massive particle production. We have shown how the constraints from energy conservation can be satisfied in all channels as a part of the QCD factorization theorem.

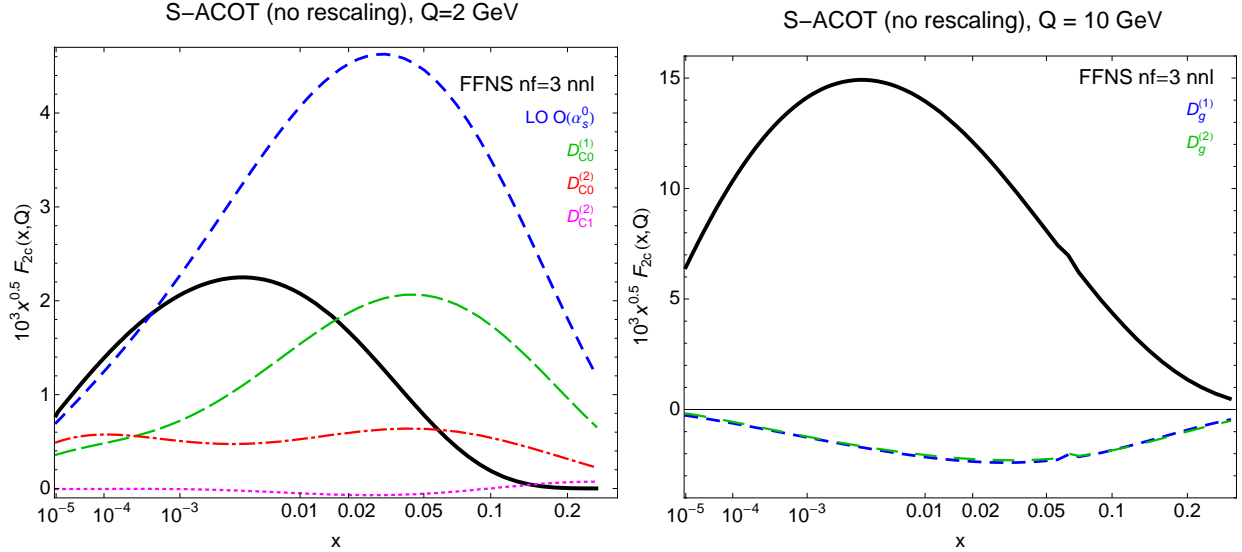


FIG. 8: Same as Fig. 7, in the S-ACOT scheme without rescaling.

These constraints are included in the definition of the  $Z$  operation in the Collins' proof of QCD factorization by rescaling the partonic momentum fraction in flavor-excitation Wilson coefficients. The S-ACOT- $\chi$  scheme thus realizes correct kinematical dependence solely by the means of the QCD factorization theorem and momentum conservation.

Schemes of the ACOT family differ only in mass-dependent terms in heavy-quark Wilson coefficient functions. PDFs are given by the same operator matrix elements in all schemes, such as Eq. (3). Estimates of these PDFs from global fits converge to unique universal functions as order of the QCD coupling increases. Convergence is the fastest in the S-ACOT- $\chi$  scheme.

At NNLO, dependence of S-ACOT- $\chi$  predictions on the factorization scale and other tunable parameters is reduced compared to NLO. Cancellations between classes of Feynman diagrams are stabilized once NNLO terms are included. The derivation of S-ACOT- $\chi$  predictions is simpler than in some other GM schemes, as it is carried out by assuming a unique number of active flavors ( $N_f$ ) and one set of universal PDFs in every  $Q$  range [12, 29]. It is minimal, in the sense that it does not impose conditions on the  $Q$  derivatives of structure functions [14] or introduce a damping factor [18]. Yet, after the NNLO terms are included, the S-ACOT- $\chi$  predictions result in good agreement with the other GM schemes. As the default heavy-quark scheme of CTEQ PDF analyses, the S-ACOT- $\chi$  scheme is going to play a crucial role in global fits at NNLO.

#### Acknowledgments

Many ideas in this paper were inspired by Wu-Ki Tung. We thank J. Smith for providing the computer code for computing massive NNLO DIS cross sections and for helpful comments on this work, and J. Huston, F. Olness, J. Pumplin, D. Stump, and other CTEQ members for useful discussions. MG and PMN appreciate stimulating communications with S. Alekhin, J. Blümlein, A. Cooper-Sarkar, S. Forte, A. Mitov, J. Rojo, and R. Thorne. This work was supported in part by the U.S. DOE Early Career Research Award DE-SC0003870; by

the U.S. National Science Foundation under grant PHY-0855561; by the National Science Council of Taiwan under grants NSC-98-2112-M-133-002-MY3 and NSC-99-2918-I-133-001; and by Lightner-Sams Foundation. CPY appreciates hospitality of the National Center for Theoretical Sciences in Taiwan, where a part of this work was done.

- 
- [1] W. K. Tung et al., JHEP **02**, 053 (2007).
  - [2] M. A. G. Aivazis, J. C. Collins, F. I. Olness, and W.-K. Tung, Phys. Rev. **D50**, 3102 (1994).
  - [3] J. C. Collins, Phys. Rev. **D58**, 094002 (1998).
  - [4] M. Kramer, 1, F. I. Olness, and D. E. Soper, Phys. Rev. **D62**, 096007 (2000).
  - [5] W.-K. Tung, S. Kretzer, and C. Schmidt, J. Phys. **G28**, 983 (2002).
  - [6] H.-L. Lai et al., Phys. Rev. **D82**, 074024 (2010).
  - [7] P. M. Nadolsky et al., Phys. Rev. **D78**, 013004 (2008).
  - [8] J. Pumplin et al., Phys. Rev. **D80**, 014019 (2009).
  - [9] S. Moch and M. Rogal, Nucl. Phys. **B782**, 51 (2007).
  - [10] S. Moch, J. A. M. Vermaseren, and A. Vogt, Nucl. Phys. **B813**, 220 (2009).
  - [11] M. Buza and W. L. van Neerven, Nucl. Phys. **B500**, 301 (1997).
  - [12] M. Buza, Y. Matiounine, J. Smith, and W. L. van Neerven, Eur. Phys. J. **C1**, 301 (1998).
  - [13] A. Chuvakin, J. Smith, and W. L. van Neerven, Phys. Rev. **D61**, 096004 (2000).
  - [14] R. S. Thorne and R. G. Roberts, Phys. Lett. **B421**, 303 (1998).
  - [15] R. S. Thorne and R. G. Roberts, Phys. Rev. **D57**, 6871 (1998).
  - [16] R. S. Thorne, Phys. Rev. **D73**, 054019 (2006).
  - [17] S. Alekhin, J. Blumlein, S. Klein, and S. Moch, Phys. Rev. **D81**, 014032 (2010).
  - [18] S. Forte, E. Laenen, P. Nason, and J. Rojo, Nucl. Phys. **B834**, 116 (2010).
  - [19] J. Sanchez Guillen, J. Miramontes, M. Miramontes, G. Parente, and O. A. Sampayo, Nucl. Phys. **B353**, 337 (1991).
  - [20] W. L. van Neerven and E. B. Zijlstra, Phys. Lett. **B272**, 127 (1991).
  - [21] E. B. Zijlstra and W. L. van Neerven, Phys. Lett. **B273**, 476 (1991).
  - [22] R. Thorne, PoS **DIS2010**, 053 (2010), arXiv:1006.5925.
  - [23] S. Alekhin, S. Alioli, R. D. Ball, V. Bertone, J. Blumlein, et al. (2011), arXiv:1101.0536.
  - [24] R. Plačakytė (2010), talk at the PDF4LHC meeting, <http://indico.cern.ch/materialDisplay.py?contribId=6&sessionId=2&materialId=slides&confId=103872>.
  - [25] F. Aaron et al. (H1 and ZEUS Collaboration), JHEP **1001**, 109 (2010).
  - [26] E. Laenen, S. Riemersma, J. Smith, and W. L. van Neerven, Nucl. Phys. **B392**, 162 (1993).
  - [27] S. Riemersma, J. Smith, and W. L. van Neerven, Phys. Lett. **B347**, 143 (1995).
  - [28] B. Harris and J. Smith, Nucl.Phys. **B452**, 109 (1995).
  - [29] M. Buza, Y. Matiounine, J. Smith, and W. van Neerven, Phys.Lett. **B411**, 211 (1997).
  - [30] I. Bierenbaum, J. Blumlein, and S. Klein, Nucl.Phys. **B780**, 40 (2007).
  - [31] I. Bierenbaum, J. Blumlein, and S. Klein, Phys.Lett. **B672**, 401 (2009).
  - [32] M. A. G. Aivazis, F. I. Olness, and W.-K. Tung, Phys. Rev. **D50**, 3085 (1994).
  - [33] P. M. Nadolsky and W.-K. Tung, Phys. Rev. **D79**, 113014 (2009).
  - [34] E. Witten, Nucl. Phys. **B104**, 445 (1976).
  - [35] S. Moch, J. A. M. Vermaseren, and A. Vogt, Phys. Lett. **B606**, 123 (2005).
  - [36] J. Vermaseren, A. Vogt, and S. Moch, Nucl.Phys. **B724**, 3 (2005).
  - [37] W. A. Bardeen, A. J. Buras, D. W. Duke, and T. Muta, Phys. Rev. **D18**, 3998 (1978).



- [38] G. Altarelli, R. K. Ellis, and G. Martinelli, Nucl. Phys. **B143**, 521 (1978).
- [39] B. Humpert and W. L. van Neerven, Nucl. Phys. **B184**, 225 (1981).
- [40] M. Buza, Y. Matiounine, J. Smith, R. Migneron, and W. van Neerven, Nucl.Phys. **B472**, 611 (1996).
- [41] S. L. Adler, Phys. Rev. **143**, 1144 (1966).
- [42] G. Altarelli, Phys. Rept. **81**, 1 (1982).
- [43] Y. L. Dokshitzer, G. Marchesini, and B. R. Webber, Nucl. Phys. **B469**, 93 (1996).
- [44] R. Brock et al. (CTEQ), Rev. Mod. Phys. **67**, 157 (1995).
- [45] <http://hep.pa.msu.edu/cteq/public/SACOTNNLO2011/>.
- [46] W. Giele et al. (2002), hep-ph/0204316.
- [47] M. R. Whalley, D. Bourilkov, and R. C. Group (2005), hep-ph/0508110; <http://hepforge.cedar.ac.uk/lhapdf/>.
- [48] G. P. Salam and J. Rojo, Comput. Phys. Commun. **180**, 120 (2009).
- [49] A. D. Martin, W. J. Stirling, R. S. Thorne, and G. Watt, Eur. Phys. J. **C63**, 189 (2009).
- [50] J. Andersen et al. (SM and NLO Multileg Working Group) (2010), p. 110, arXiv:1003.1241.